ELSEVIER

Surface Science 500 (2002) 1–27

SURFACE SCIENCE

www.elsevier.com/locate/susc

Surfaces: a playground for physics with broken symmetry in reduced dimensionality

E.W. Plummer [a,b,*], Ismail [a,b], R. Matzdorf [c], A.V. Melechko [a,b], J.P. Pierce [a,b], Jiandi Zhang [d]

[a] *Department of Physics and Astronomy, The University of Tennessee, 401 A.H. Nielsen Physics Building, Knoxville, TN 37996-1200, USA*

[b] *Oak Ridge National Laboratory (ORNL), Oak Ridge, TN 37831-6057, USA*

[c] *Universität Würzburg, Experimentelle Physik IV, Am Hubland, 97074 Würzburg, Germany*

[d] *Department of Physics, Florida International University, Miami, FL 33199, USA*

Received 4 January 2001; accepted for publication 11 July 2001

Abstract

With our crystal ball in front of us, we attempt to articulate the opportunities and challenges for a surface physicist in the beginning of the new millennium. The challenge is quite clear: to use the unique environment of a surface or interface to do fascinating physics, while taking full advantage of the skills the community has developed over the last 30 years. The opportunities appear to be endless! In this age of Nanotechnology where the promise is to shape the world atom by atom, leading to the next industrial revolution [Nanotechnology: shaping the world atom by atom, National Science and Technology Council, Committee on Technology, 1999], surface science should be at the very forefront of both technological and scientific advances. The smaller objects become, the more important their surfaces become. In this article we focus on the role of a surface physicist in the emergence of nanoscale collective phenomena in complex materials.

Keywords: Surface structure, morphology, roughness, and topography; Surface defects; Magnetic phenomena (cyclotron resonance, phase transitions, etc.)

1. Introduction

As we enter the new millennium the international science agenda is focused on nanoscale science and technology [1,2]. We begin the ''age of designer materials,'' when complex materials are designed to have desired properties, with both basic and technological applications. Some present day examples include artificially patterned structures, forever-smaller integrated circuits, magnetic storage devices, composite materials, polymer blends, doped transition-metal oxides, self-assembling nanostructures, molecular electronics, etc. This volume is intended to guide a surface or interface scientist into this new world, spanning all of the basic disciplines (chemistry, physics,

* Corresponding author. Address: Department of Physics and Astronomy, The University of Tennessee, 401 A.H. Nielsen Physics Building, Knoxville, TN 37996-1200, USA. Tel.: +1-865-974-3055; fax: +1-865-974-3895.

E-mail address: eplummer@utk.edu (E.W. Plummer).

0039-6028/01/$ - see front matter
PII: S0039-6028(01)01565-5

biology, etc.), and extending to the exciting areas of technological applications. This article concerns a narrow aspect of surface science, specifically the prospects for a surface scientist in the world of condensed matter physics (CMP). There are other exciting, more global or cosmological aspects of surface science covered in this volume by Broglia (*The surface of compact systems*: *from nuclei to stars*) [3], Greenberg (*Cosmic dust and other origins*) [4], Herbst and Williams (*It's a dusty universe*: *surface science in space*) [5], and Madey et al. (*Far-out surface science*: *radiation-induced surface processes in the solar system*) [6].

2. Themes in modern condensed matter physics

In this section we briefly outline the general themes in CMP as we enter the new millennium. The idea is to understand where CMP is going so that a surface physicist can engage, participate, and contribute. There are three general thematic areas that have emerged in the last several years, which will guide the general direction of CMP in the next decade.

(i) nanoscale science and technology,
(ii) complex systems,
(iii) functional materials.

Worldwide, *Nano-scale Science*, *Nano Engineering*, *and Nano Technology* have become the buzzwords for discussing the future of materials sciences. It seems that 'nanocenters' are appearing on university and government campuses at a faster rate than daycare centers. The obvious reason for this interest is stated in the Department of Energy (DOE) report, Nanoscale Science, Engineering and Technology Research Direction [2]. "The reason that nanoscale materials and structures are so interesting is that size constraints often produce qualitatively new behavior. We now understand, in a general way, that when the sample size, grain size, or domain size becomes comparable with the specific physical length scale such as the mean free path, the domain size in ferromagnets or ferroelectrics, the coherence length of phonons, or the correlation length of a collective ground state as in superconductivity, then the corresponding physical phenomenon will be strongly affected. Although such changes in behavior can be the dominant effects in nanoscale structures, we still have remarkably little experience or intuition for the expected phenomena and their practical implication, except for electronic systems. The physics, chemistry and biology of phenomena occurring in nanoscale systems is effectively a new subject with its own set of physical principles, theoretical descriptions, and experimental techniques, which we are only in the process of discovering. Thus, there is an urgent need for broadly based investigations of the physical phenomena associated with confined systems, especially in materials and structural contexts where the implications are not at all well understood."

The DOE, Office of Science Workshop on Science for the 21st Century discussed the many facets of *complex systems*. This report [7] outlines the opportunities and challenges for the future. "As we look to the next century, we find science and technology at yet another threshold: the study of simplicity will give way to the study of *complexity* as the unifying theme."

The new millennium will take us into the world of complexity. Here, simple structures interact to create new phenomena and assemble themselves into devices. Here also, complicated structures can be designed atom by atom for desired characteristics. With new tools, new understanding, and a developing convergence of the disciplines of physics, chemistry, materials science, and biology, we can build on our 20th century successes and begin to ask and solve questions that were, until the 21st century, the stuff of science fiction.

Complexity can take many forms, so the identification of five emerging themes by the DOE workshop participants is useful as an organizational guide. The five themes are

- *Collective phenomena*—Can we achieve an understanding of collective phenomena to create materials with novel, useful properties?
- *Materials by design*—Can we design materials having predictable, and yet often unusual properties?

- *Functional systems*—Can we design and construct multicomponent molecular devices and machines?
- *Nature's mastery*—Can we harness, control, or mimic the exquisite complexity of nature to create new materials that repair themselves, respond to their environment, and perhaps even evolve?
- *New tools*—Can we develop the characterization instruments and the theory to help us probe and exploit this world of complexity?

In our opinion, the theme of Functional Systems is important enough to be broadened in content and listed as one of the three main thematic areas of CMP; Functional Materials.

For a physicist an interesting material has to do something. It has to be a *Functional Material*. It does not make any sense to fabricate a nanoscale material that is complex yet does nothing when its environment is changed. In physiological terms, we would like to design a material that is "schizophrenic" in that it develops a multitude of different personalities that appear in response to a prescribed stimulus. In scientific terms we want a material that has many and varied competing ground states so that an external stimulus (heat, pressure, electric field, magnetic field, etc.) can be used to switch its 'personality.' In the remaining portion of this section we illustrate that there are families of materials that allow you to "have your cake and eat it at the same time." Their properties are not only dictated by what occurs on a nanoscale, but they are also complex and wildly schizophrenic.

Before proceeding, it is important to understand that underlying all three of the thematic areas of modern CMP is our ability to synthesize, fabricate, or process advanced materials. The materials community must develop special tools to synthesize [8, p. 135] and characterize complex systems in order to make rapid progress. This is an area in which the surface science community can excel; growing and characterizing novel nanophase material structures. We are experts in this endeavor!

Although there are many aspects of complexity, we begin by talking about complex structures, and designer materials that exhibit nanoscale behavior, either because of *nature's mastery*, man's design, or a combination of both. Fig. 1 schematically illustrates four different forms of complex materials; (a) soft or biomaterials, (b) transition-metal oxides (TMOs), (c) artificially fabricated structures, and (d) designed quantum objects. Castner/Ratner (*Biomedical surface science*: *foundations to frontiers*) [9], Fahlman/Salaneck (*Surfaces and interfaces in polymer-based electronics applications*) [10], Kasemo (*Biological surface science*) [11], Norskov and Rod (*The surface science of Enzymes*) [12], Safran (*Statistical thermodynamics of soft surfaces*) [13], and Tirrell et al. (*The role of surface science in bioengineered materials*) [14], all describe the role of surface science in soft materials in their articles in this volume. Bader (*Magnetism in low dimensionality*) [15], Shen/Kirschner (*Tailoring magnetism in artificially structured materials*: *the new frontier*) [16], and Arthur (*Molecular beam epitaxy*) [17] describe phenomena in two dimensional artificially structured materials like those shown in Fig. 1(c). Dai (*Carbon nanotubes*: *growth*, *properties and applications in surface science*) [18], Freund (*Clusters and islands on oxides*: *from catalysis via electronics and magnetism to optics*) [19], Eberhardt (*Clusters as new materials*) [20], and Naumovets/Zhang (*Fidgety particles on surfaces* [21]. *How do they jump*, *walk*, *group*, *and settle in virgin areas*?) all describe artificially structured quantum objects on a surface as depicted in Fig. 1(d). In this article we focus on the new physics that can occur at the surfaces of chemically or electronically complex materials such as shown in Fig. 1(b).

The high-temperature superconductors offer examples of complexity, reduced dimensionality, and broken symmetry. Here, we use the term "reduced dimensionality" to denote systems in two, one, and zero dimensions. The dimensionality is dictated by the size in a certain direction of the object compared to an appropriate length scale for the phenomena being discussed. If one dimension of the sample is small compared to this length parameter, then the object is two dimensional (2D). Fig. 2 is an artist's view of the high-T_c material $HgBa_2Ca_2Cu_3O_{8+x}$ [7,22]. This material has one of the highest superconducting temperatures

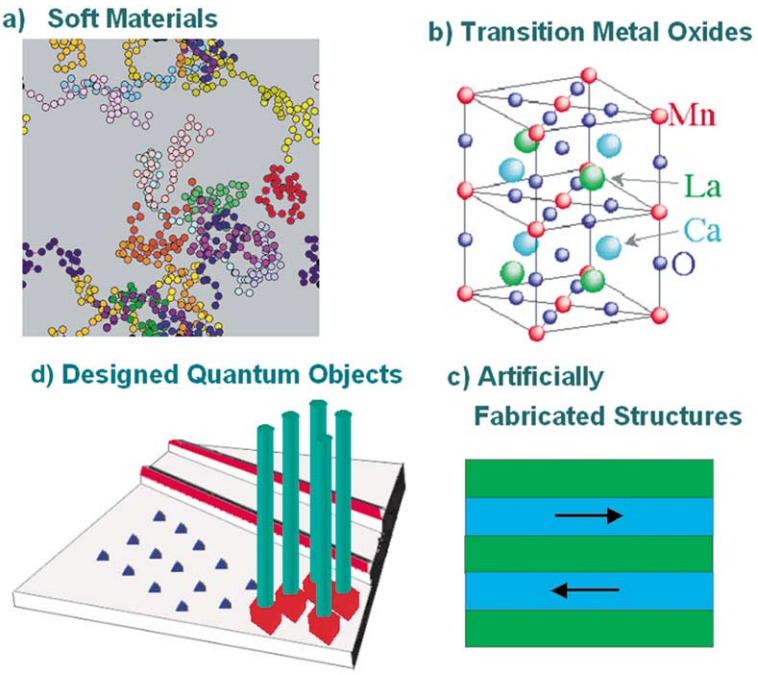

Fig. 1. Schematic illustrations of different important types of complex materials that will be encountered in this special issue of Surface Science. (a) Soft materials, like polymers and biomaterials, are made of interconnected chains of many kinds of molecules. Condensed matter physicists are only beginning to learn how to exploit the unique properties of these immensely complex systems. (b) In ordered materials that are made of many elements, like the TMOs, complex chemical composition leads to highly tunable electronic, magnetic, and structural properties. This figure shows the structure of the perovskite $La_{1-x}Ca_xMnO_3$, where x can range from 0 to 1. (c) 2D complex sandwich structures made of magnetic (blue) and nonmagnetic (green) layers have electronic properties that change drastically in the presence of a magnetic field. These materials have already proven useful in magnetic data reading/writing devices. (d) It has only recently become possible to fabricate quantum objects like nanowires (red) and nanocolumns (green) and quantum dots (blue). These objects are built on length scales which are similar to or smaller than the characteristic lengths over which many fundamental electronic and magnetic interactions occur, which should lead to exotic behavior.

recorded (133.5 K), when optimally doped with oxygen ($x \sim 0.14$) [22]. Doping generally refers to the addition of a small amount of an element that will give or take charge from the host lattice. Conventional wisdom says that the superconductivity occurs in the central CuO_2 plane (shaded with green in the figure), so this is really a 2D system. The parent compound ($x = 0$) is not a superconductor but when excess O is incorporated into the Hg–O lattice it pulls charge out of the CuO_2 plane (called hole doping, because O takes charge from the CuO_2 plane leaving a hole) and drives the material into the superconducting state. Doping with O breaks the translational symmetry of the crystal, creating nanoscale inhomogeneities (see the example in Section 3.3), that may be intimately related to the origin of superconductivity in these materials. A comparison of the coherence length in the superconducting phase dramatically illustrates the difference between these complex oxides and ordinary superconductors. The easiest way to define the coherence length is as the minimum spatial extent of a transition layer between the normal and superconducting states. For a normal superconductor like Al ($T_c = 1.14$ K) the coherence length is isotropic and very long ($\sim 10^4$ Å), while for this material it is anisotropic, and much shorter; $\sim$10 Å perpendicular to the CuO_2 plane and $\sim$50 Å in the plane. The perpendicular coherence length is less than the 15.86 Å lattice spacing. The inherent 2D-layered nature of the high-T_c materials, coupled with the short inter-

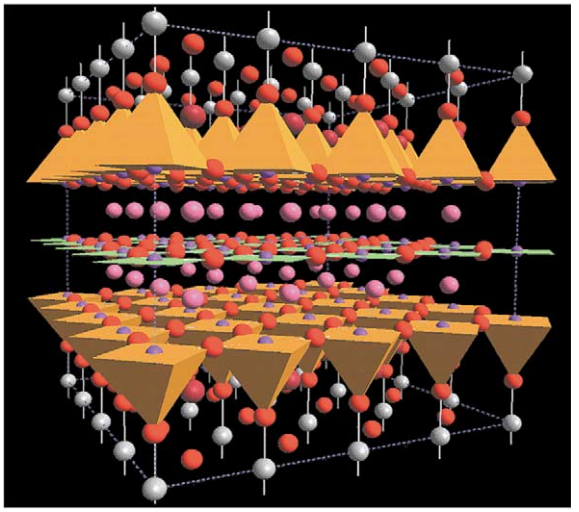

Fig. 2. Artistic view of the crystal structure of the high-temperature superconductor $HgBa_2Ca_2Cu_3O_{8+x}$ [7], showing highly 2D (layered) character. The color code is: silver for Hg, purple for Cu, red for O, pink for Ca and dark red for Ba. The orange pyramids present the appropriate portion of CuO_6 octahedra. The lattice spacing in the vertical direction is 15.86 and 3.86 Å in the plane.

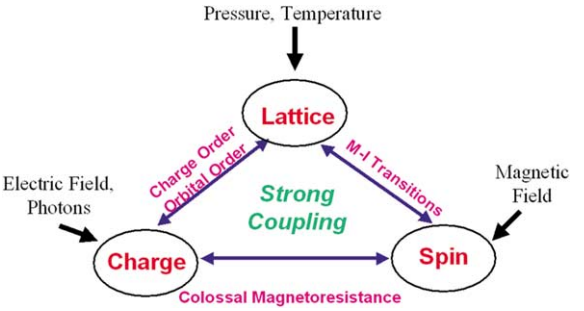

Fig. 3. Artistic representation of a highly "functional material." The electronic, spin and lattice degrees of freedom are tightly coupled, leading to dramatic responses to external probes such as temperature, pressure, and electric or magnetic fields. For example, the application of a magnetic field can shift the M–I and magnetic transition to a different temperature, thus creating a drastic change of the resistivity (i.e., CMR behavior). The application of a light beam (electric field) can melt the charge/orbital ordered insulating state (described later) creating a ferromagnetic metal.

planar coherence length, makes them amenable to investigation using conventional surface probes such as angle-resolved photoemission and scanning tunneling microscopy (STM). There is always the prospect that a clever surface scientist can engineer the growth of a unique superconducting thin film, and perhaps even fabricate one that has a transition temperature above room temperature.

High-temperature superconductors are only one class of a set of materials usually referred to as 'highly correlated electron systems.' A special issue of Science (*correlated electron systems*), April 21, 2000, was devoted to this subject [23]. The commonality these materials have is the dominant role played by electron–electron interaction that goes far beyond our conventional wisdom. No current textbook theory can explain the exotic behavior of these materials [24]. Examples of these highly correlated electron systems are TMOs, heavy fermion metals, organic charge transfer compounds, and 1D and 2D electron gas systems [25]. The TMOs are characterized by a strong coupling between the structural, electronic, and magnetic properties leading to richness in their physical properties, which can be tuned by doping. In this case the word doping is really not correct because the properties are actually tuned by chemical substitution. For example, divalent Ca is substituted for trivalent La in Fig. 1(b). "With this strong correlation, even a small change in an external parameter can have a drastic effect on the system's ground state, changing the electronic and/or magnetic phase of the material from one ground state to another" [24]. Fig. 3 illustrates schematically the effect of this close coupling of spin, charge and the lattice degrees of freedom. In the science compass section of the special issue of Science, Birgeneau and Kaster comment, "Clearly, highly correlated electron systems present us with profound new problems that almost certainly will represent deep and formidable challenges well into this new century [25]."

To illustrate the range of dimensionality in the TMOs, Fig. 4 displays the structure of the Ruddlesden–Popper (RP) series described by the general formula $(A_{1-x}B_x)_{n+1}M_nO_{3n+1}$. In these compounds A is usually a trivalent rare-earth element, B is a divalent alkaline-earth element, and M is a transition-metal ion that can have several different valences. The structure of the RP phases is composed of n consecutive perovskite layers

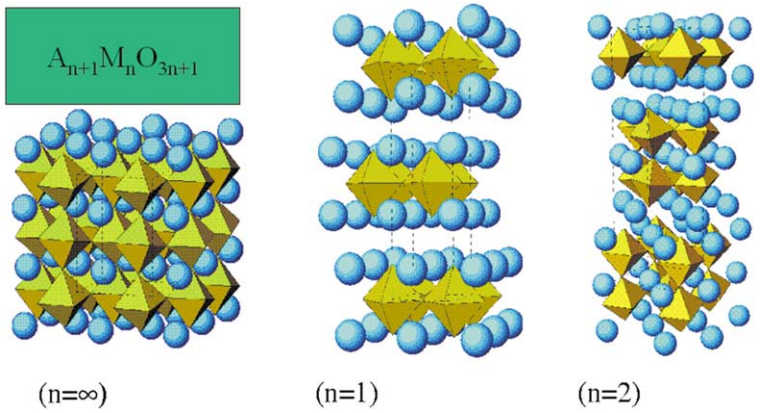

Fig. 4. Artistic view of three members of the RP series ($A_{n+1}M_nO_{3n+1}$) for $n = 1$, 2, and ∞. The A ions are the large-blue spheres with the MO_6 octahedra displayed as the light-green solid object. The structural properties of the $n = 1$ and $n = 2$ phases are clearly low dimensional and are expected to lead to highly anisotropic physical properties, while the $n = \infty$ structure is 3D.

(AMO_3) alternating with rock salt layers so that their formula can be represented by (AO)-(AMO_3)$_n$, where n represents the number of connected layers of vertex sharing MO_6 octahedra (green octahedra in Fig. 4). $n = 1$ is a 2D-layered material with only one layer of octahedra. $n = 2$ has two connected layers of octahedra. As n increases the materials become more 3D in character with $n = \infty$ being the perovskite structure. As an example of the close coupling in these materials consider the perovsike $La_{1-x}Ca_xMnO_3$ shown in Fig. 1(b). The ground state of the parent compound $LaMnO_3$ is an antiferromagnetic (adjacent spins pointing in opposite directions) insulator, but as the concentration of Ca is increased the ground state dramatically changes. Looking at the formal valence of this compound leads to the following representation, $La^{3+}_{1-x}Ca^{2+}_xMn^{3+}_{1-x}Mn^{4+}_xO^{2-}_3$. Increasing the Ca concentration changes the average valence of the Mn, leading to an array of different ground states which are described as ferromagnetic-ordered (FM) metal, charge-ordered insulator (explained later), canted-antiferromagnetic insulator, etc. [26].

When an external stimulus is applied, these materials exhibit quite remarkable changes (Fig. 3) because the energies separating the ground state from quite different excited state configurations are small. Fig. 5 illustrates several commonly observed cooperative phenomena. In Fig. 5(a) a coupled magnetic–electronic transition occurs with changing temperature in the perovskites ($A_{1-x}B_x$-MO_3), for a doping of $x \sim 0.3$. The ground state is a FM metal that changes to a paramagnetic (PM) insulator as the temperature is raised. The signature of a metal is a resistivity that increases as the temperature rises, while the resistivity of a semiconductor or insulator decreases with increasing temperature. The transition temperature for this coupled transition depends on the size and electronic properties of the divalent and trivalent components, ranging from ~60 K for $Pr_{0.7}Ca_{0.3}$-MO_3 to ~370 K for $La_{0.7}Ca_{0.2}MO_3$. The transition temperature for a given material depends on the strength of the applied magnetic field, moving to lower temperature as the field increases. This produces what is known as colossal magnetoresistance (CMR), as shown in Fig. 5(b). Magnetoresistance is the change in the resistance $\Delta R/R$ of a material in the presence of an applied magnetic field. This is normally on the order of a few percent. The phrase giant magnetoresistance (GMR) is used to describe the magnetoresistance in artificially layered metal films (see Fig. 1(c)) and can be as large as 100% (see Section 3.1). CMR in the TMOs can be as large as 10^5. When light, either from X-rays or a laser, is incident on some of the TMOs, a startling transition occurs from an antiferromagnetic insulator to a ferromagnetic metal, as depicted in Fig. 5(c) [27–29].

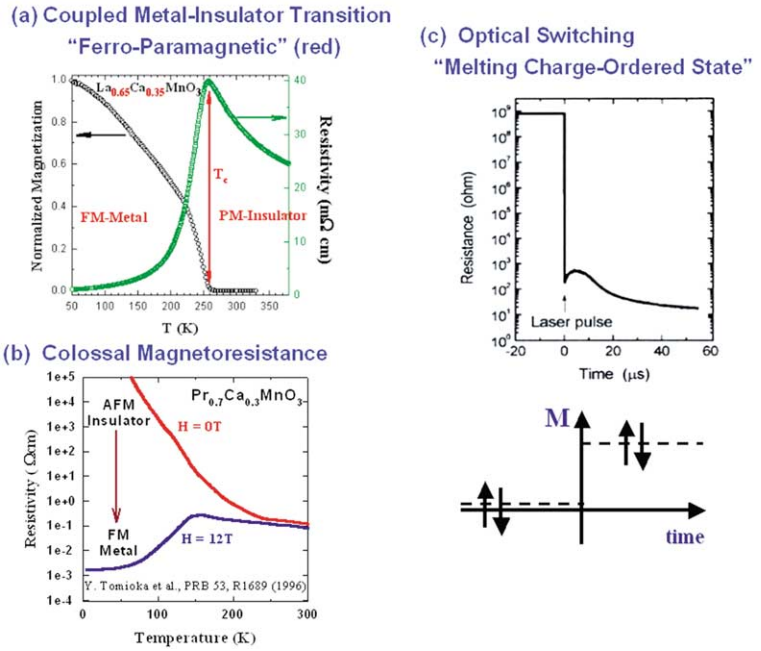

Fig. 5. Illustration of a few of the macroscopic collective phenomena seen in TMOs. (a) A coupled FM to PM phase transition (based on the measurement of magnetization vs. temperature) and a M–I transition (based on the change of resistivity vs. temperature) in $La_{0.65}Ca_{0.35}MnO_3$. (b) CMR, i.e., a drastic decrease in resistivity by applying an external magnetic field is observed in $Pr_{0.7}Ca_{0.3}MnO_3$. The change in resistivity with applied field is a function of the sample temperature, going to zero at room temperature. (c) Optical switching in $Pr_{0.7}Ca_{0.3}MnO_3$, where the physical properties change dramatically with the exposure to light. In this case the material can switch its charge-ordered insulating state with an antiferromagnetic spin structure (nearest neighbor spins are antiparallel with lower magnetization) to its charge-disordered metallic state with a ferromagnetic spin structure (nearest neighbor spins are parallel with higher magnetization). The change in resistivity when the laser pulse hits the sample is shown in the top and the spin alignment below, both as a function of time with $t = 0$ at the time when the laser was pulsed [26–29].

Creating a surface by cleaving a TMO single crystal is a controlled way to disturb the coupled system (spin, charge, and lattice) by breaking the symmetry without changing the stoichiometry. The unique environment at the surface could produce new phenomena, while providing a fresh approach to the study of the spin, charge, and lattice coupling in these complex materials (see Section 3.3). Furthermore, the influence of surfaces and interfaces on thin-film properties is of technological interest for the design of TMO devices.

There is a paradigm shift occurring in CMP, from detailed studies of model systems to embracing the importance of complexity. Associated with complexity is the emergence of new phenomena and the realization that controlled synthesis is the enabler for their discovery and understanding. Discovery of new phenomena requires exploring the frontiers of complexity in all of its forms. One such new phenomenon is electronic nanoscale phase separation in these highly correlated systems [30–38]. In a conventional solid, the ion cores create the symmetry of the solid and the electronic charge density has the same symmetry. In some highly correlated systems there can be static and dynamic variations in the charge density that does not follow the symmetry of the ion cores. The best-known observation of this phenomenon is the striped phases in the high-T_c superconductors reported by Tranquada et al. [30] (see Fig. 6(a)), which has lead to a virtual zoo of predictions on new nanophase separations in TMOs [32–38]. There seems to be a general trend in these systems toward an intrinsic nanophase separation close to the phase boundaries in

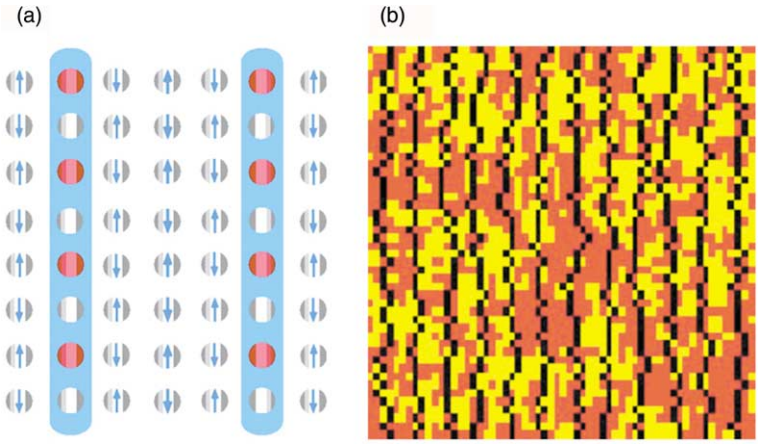

Fig. 6. (a) Theorists view [32] of the static stripe phase of the high-T_c superconductor $La_{01.475}Nd_{0.4}Sr_{0.125}CuO_4$ [30]. Here, the charge is largely confined to the channels shaded in blue. The average charge density along the stripe of +e per two sites is indicated by alternating red and silver circles. Blue arrows indicate magnitude of the magnetic moment on sites containing spins. The strip is an antiphase boundary for the antiferromagnetic order; in the absence of the stripe, the first and third column from the left would have the same spin orientation, not an opposite one. The oxygen ions are not shown. (b) Theoretical image of fluctuating quantum stripes (lines of black dots) moving through a quantum antiferromagnet (red/yellow background) from an imaginary time slice of a quantum Monte Carlo simulation. In the classical limit the background would be, say, uniformly red, corresponding to a simple antiferromagnet. Here the yellow patches represent spin fluctuations [38]. In both (a) and (b) the length scale is in nanometers.

temperature, doping concentration, or magnetic field. Although there is no direct proof that striped phases dictates the properties of high-T_c materials [27], there is growing evidence that dynamic mixed nanophases (see Fig. 6(b)) are an integral part of the CMR behavior [34]. The length scales of the phase separated regions are in the nanometer range, involving fluctuations of charge, spin, and orbital orientation [23,31,32]. Current examples of direct observations of electronic inhomogeneities on the surfaces of these highly correlated electron systems are included in Section 3.3.

Fig. 7 is a picture representing orbital, charge, and spin ordering that occurs in perovskites [23,26,31]. This is a specific example for the quarter-doped sample ($x = 0.25$) $A_{0.75}B_{0.25}MnO_3$, in which there is a 3/1 ratio of Mn^{3+} to Mn^{4+} caused by doping. In principle, the divalent ions (B) are randomly distributed on the blue ball lattice in Fig. 4, but local or long-range charge ordering of the Mn ions can occur at low-temperatures. This is shown in Fig. 7 by having each of the Mn^{4+} ions shown as light and dark red balls surrounded by six Mn^{3+} ions (with light and dark green orbital lobes). Orbital ordering occurs when the occupied orbitals in the Mn^{3+} ions align themselves with respect to the Mn^{4+} as shown by the green orbital. Spin ordering occurs with ferromagnetic coupling between the spin $-3/2$ Mn^{4+} and the spin-2 Mn^{3+} nearest neighbors, as shown in the right-hand panel of Fig. 7. The spin, orbital, or charge ordering can be static or dynamic, short range (light green) or long range depending upon the details of the coupling in the system.

Given the high sensitivity of these materials to their local environment, it is likely that in some cases their surfaces could behave totally different from the bulk. It takes very little imagination on the part of a surface scientist to envision charge-, orbital- or spin-ordered surface states on these materials, or the inverse in which the bulk is a charge-ordered antiferromagnetic insulator and the surface is a ferromagnetically ordered metal. An example, which illustrates the possibilities, is described in Section 3.3.

We have learned that one key characteristic of complex materials is that it is possible to create spectacular, new phenomena simply by adding new components to a given material. This was illustrated by the discovery of high-temperature

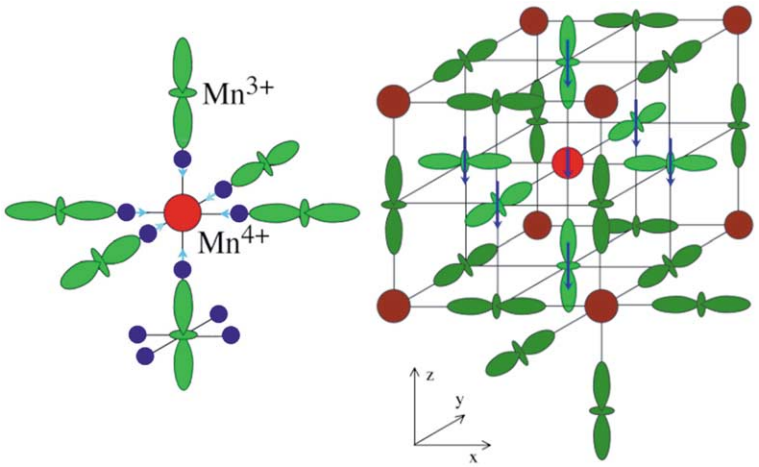

Fig. 7. Schematic representation of the charge, spin and orbital ordering in a perovskite $A_{0.75}B_{0.25}MnO_3$ where A represents trivalent rare-earth ions and B sites are occupied divalent alkaline-earth doped ions [31]. Doping divalent ions creates a Mn mixed-valent configuration, with 25% Mn^{4+} (light/dark red balls) and 75% Mn^{3+} (light/dark green lobes representing the electron orbitals), exhibiting spin, charge, and orbital ordering below a critical temperature. The basic buiding block for the charge/orbital ordering is shown in the cluster in the left panel, a Mn^{4+} ion with spin (3/2) is surrounded by six short bond length oxygen (O) atoms (purple circles) and six Mn^{3+} ions (green orbitals) with spin 2 ferromagnetically coupled to the central Mn^{4+}. The fourth 3d electrons in the Mn^{3+} ions occupy the lobes as drawn, all pointing toward the central Mn^{4+} ion and to local long Mn^{3+}–O bond lengths. The right panel shows the charge/orbital ordered cluster embedded in the host material. It is the charge and orbital ordering which results in the peculiar magnetic structure, in this case with ferromagnetic clusters which can be antiferromagnetically ordered with respect to each other in the solid.

superconductivity, CMR, and conducting polymers. In the future, new phenomena will be discovered by artificially growing complex structures out-of-equilibrium as depicted in Fig. 1(c) and (d). The objective will be to control the *coupling* of cooperative phenomena, such as, the coupling between magnetic ordering and a structural transition, or between magnetism and electrical conductivity or superconductivity. What we have learned is that complex or composite systems do not behave simply as linear combinations of the properties of the parent materials. In a much earlier time, Sir Arthur Eddington aptly and eloquently described this situation in saying

> *We used to think if we knew one, we knew two, because one and one are two. We are finding that we must learn a great deal more about* '***and***'.

For complex materials, we must understand the way in which "and" governs all of the factors that combine to produce dramatic new phenomena. One thing that we have learned is that complexity is a Fountain of Youth. Pushing the *frontiers* of chemically and structurally complex materials will always cause new phenomena to emerge. Consequently, the subjects of complexity and cooperative phenomena are *fundamental*, *long-term* interests of science and society. Some time ago Phil Anderson presciently observed that,

> *...at each new level of complexity, entirely new properties appear, and the understanding of these behaviors requires research which I think is as fundamental in its nature as any other* [39]

A survey of new phases of matter and recent Nobel Prizes clearly illustrates the trend. Table 1 was taken from the 1999 APS centennial presentation by Piers Coleman, titled "An Unfinished Revolution." The table has been updated with recent discoveries and awards. The 2000 Nobel

Table 1
List of recently discovered new phases of matter and accompanying Nobel Prizes

Nobel Prize Year	New phases of matter	Dimensionality
	Non-Fermi liquid	3D
	Heavy fermion metals	↓
1991	Liquid crystals	↓
1987	High-T_c superconductors	↓
	CMR	↓
2000	Conducting polymers	↓
1985, 1998	Quantum Hall effect	↓
	2D Metal–insulator transition	↓
	Quantum dots	↓
1996	C_{60}	0D

On the right is a rough measure of the dimensionality of the system.

Prize in physics to Alferov and Kroemer for developing semiconductor heterostructures used in high-speed and opto-electronics should also be included. The message is quite clear. If you want to discover a new phase of matter or win a Nobel Prize you need to embrace complex materials which exhibit collective phenomena. It should also be apparent that for devices to function in the future world of Nanotechnology, coupling of cooperative phenomena is required.

The opportunity, for those who seize it, and the risk, for those who ignore it, is that

Whoever controls the materials controls the science and the technology,

i.e., progress is materials driven. Part of this claim, that whomever controls the materials controls the science, can be substantiated by looking at the list of the 1000 most cited physicists in the period 1981 to June 1997 [40]. Of the top 10 most cited, seven were condensed matter physicists. Six of these seven make materials, ranging from superconductors to conducting polymers, QED.

We are entering a "New World of Designer Materials," designed for scientific and technological impact. There are tremendous opportunities for surface physicists, if we become engaged! These highly correlated electron systems, the questions associated with them, and the importance of nanoscale phenomena seem to be designed for a surface physicist. We have the tools and the experience to make a real impact.

3. Examples: surface physics in the world of contemporary condensed matter physics

In this section, we attempt to illustrate ways for a surface scientist to *engage* in contemporary CMP. Generally, there are three obvious paths: (1) take our surface systems and use them to illustrate the physics relevant to questions being asked by the materials physics community (map our problems onto theirs); (2) use our techniques, both experimental and theoretical, to study new materials relevant to the materials physics community; and (3) fabricate new materials with exotic behavior that attract this community.

Our challenge to you, the reader, is to construct your own version of this section. Ask yourself, "Where are the forefronts of my discipline?" Once you have this list then ask, "What can I do as a surface scientist to have an impact?" If you are a beginning graduate student looking for a thesis advisor, ask each potential advisor how he or she plans to have an impact on science or technology. If he or she does not have an answer, look for another advisor.

3.1. Magnetism in reduced dimensionality

Magnetism in reduced dimensionality illustrates every point that we emphasized in the previous sections. It is by its very nature a cooperative phenomenon involving broken symmetry. The 1990s have been referred to as the decade of magnetism in two dimensions. The important ad-

vances in this field in the last decade are due to science-driven fabrication of complex multilayered structures. Our community can be proud of its contribution to the advancement of this field. According to Bader (in Ref. [15] this volume), "The development and adaptation of surface-science techniques are responsible for enabling surface magnetism to flourish."

There are many landmark papers in this field but the discovery of GMR in 1988 [41] spurred major advances in research and development. Within a decade of the discovery of GMR, the phenomenon was adapted to a new generation of high-performance read heads in magnetic hard disks. The simplest device based on GMR is the spin valve developed by IBM and shown in Fig. 8(a). In its simplest form it can be thought of as a sandwich—a thin film of nonmagnetic material (Cu in this case) between two thin films of magnetic material (Co). The key concept is associated with the flow of electron with a spin orientation through this Co/Cu/Co sandwich as depicted in Fig. 8(b) and (c). An electron moves through a magnetic layer with relative ease when its spin is parallel to the magnetization of the layer and with relative difficulty when its spin is opposite to the magnetization direction. A magnetic material that is, for instance, magnetized in the "up" direction can be thought of as having an excess of spin-up electrons, or in the language of the condensed matter physicist, a larger density of states associated with spin up than with the spin "down" electrons. The bottom line is that spin-up electrons move through the up aligned magnetic film easier than do the spin down electrons, so the resistance is different in the two cases. When no external magnetic field is applied to the device, as in Fig. 8(b), the magnetic layers are antialigned and both spin-up and spin-down electrons are scattered equally as they try to move across the two

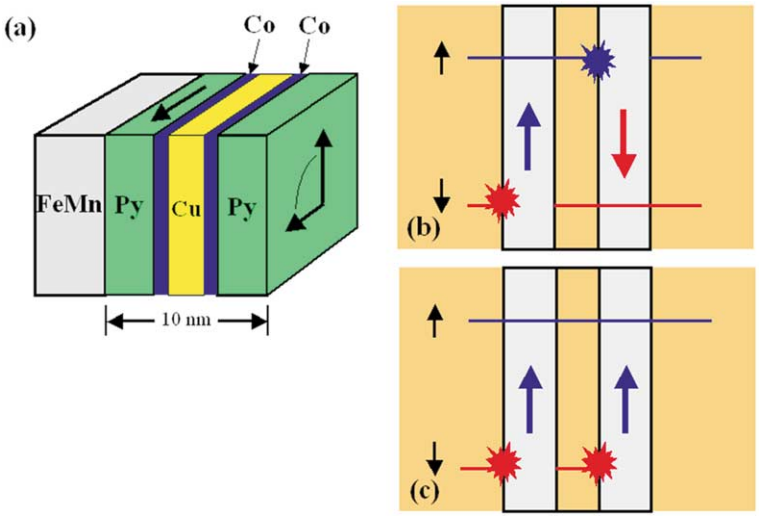

Fig. 8. GMR devices work by exploiting not only the charge of the electrons that pass through them, but also their spin. The simplest device is shown in (a), where the magnetic moment of the green permalloy (Py) layer that is furthest to the left is pinned in one direction by the neighboring FeMn layer. The magnetic moment of the Py layer that is furthest to the right responds to the magnetic field created by the magnetized domain of the "bit" of information that is written on the hard drive spinning underneath it. Passing a test current through the device immediately identifies whether the moments of the two permalloy layers of the read head are aligned (low resistance) or antialigned (high resistance), thus reading the information written on the disc. The heart of the device consists of a nonmagnetic metal film sandwiched between two magnetic layers. In this case Cu between Co layers. As shown in (b), when the magnetic moments of the magnetic layers (large red and blue arrows) are antialigned, spin up and spin down electrons (small black arrows) have an equally difficult journey through the device. When the magnetic moments of the layers are aligned as shown in (c), spin up electrons can easily pass through the device and the resistance decreases. This is the GMR effect.

magnetic layers. When a field is applied, as in Fig. 8(c), it is like opening a valve—spin-up electrons are allowed through, resulting in a large decrease in the resistance, i.e. magnetoresistance. The important length scale in this case is the spin diffusion length, which is the average distance that an electron can travel in a metal before it experiences a spin flip collision. All of the film thickness in the GMR devices must be less than the spin diffusion length for them to act as 2D systems. At room temperature, the spin diffusion lengths are roughly 40 and 20 nm in cobalt and copper, respectively.

In the Co/Cu/Co sandwich shown in Fig. 8(a) the differences in the spin-aligned (c) and spin-anti-aligned electrical conductivity is only ~20% because of the finite difference in the spin-up and spin-down density of states in Co. The dream is to fabricate a material where the spin-down density of states is zero and the spin-up density finite. This type of material is called "half-metallic," and would exhibit an infinite magnetoresistance, making an ideal switch [42].

GMR devices like the one shown in Fig. 8(a) are excellent magnetic field sensors. These devices can be manufactured on very tiny length scales (~10 nm) and are sensitive enough to read incredibly tiny magnetic bits. This has allowed IBM to manufacture the Travelstar™ disk shown in Fig. 9(a) that has a bit density of 4.1 billion bits per square inch.

The future for a surface scientist interested in magnetism is undoubtedly in designed magnetic systems in one or zero dimensions. Fig. 9(b) shows a marble model of a 1D magnetic wire array. Surface scientists can lead the way in research on magnetism in low-dimensional systems. Stepped surfaces can form ideal templates for 1D magnetic nanowires, as illustrated in Fig. 1(d). Novel growth techniques can be used to prepare zero-dimensional magnetic quantum dots (Fig. 1(d)). It should be possible to investigate in a systematic way the dimensional dependence of magnetism [15,16]. The objective is to control or to engineer the coupling in these reduced dimensional systems. For example, you could envision using more complex materials like the TMOs so that an electric field would couple to the magnetic behavior, as displayed in Fig. 5(c). There are two excellent articles in this special issue on the future of this area, by Bader [15], and by Shen/Kirschner [16].

3.2. Phase transitions in reduced dimensionality

A phase transition is a cooperative phenomenon involving the concepts of broken symmetry and dimensionality. It has long been recognized that changing the dimensionality of a system has profound effects on phenomena associated with phase transitions. For example Landau and Lifshitz have proven that long-range order cannot occur in a 1D system whose elements interact

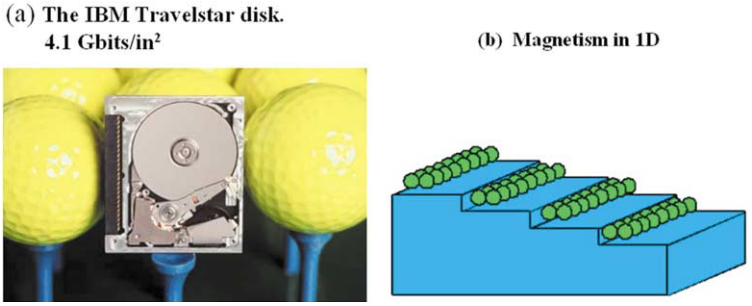

Fig. 9. (a) A photo of the Travelstar™ disc, manufactured by IBM. The disc spins as if it were on a record player and the information on it is read by a tiny GMR read head placed at the end of the "needle" of the record player. GMR read heads, like the one shown in the previous figure, can be manufactured on length scales on the order of 10 nm. The small size and high sensitivity of these devices have led to increased performance of magnetic information storage media. The disc shown above has an information storage density of 4.1 billion bits per square inch. (b) A marble model of a 1D magnetic nanowire array. By miscutting substrate surfaces to form atomic staircases, it is possible to grow parallel arrays of these nanowires using the stepped surface as a template [16].

through finite-range forces [43]. It is also anticipated that defects will play a larger role in phase transitions in low-dimensional systems [44], though microscopic evidence has been limited. This is an area where we as surface scientists should be able to have an impact on the materials community using our systems and our tools.

Historically there have been many investigations of 2D surface phase transitions. One area where immense progress has occurred is in the area of weakly bound inert gas atoms on surfaces [45]. One of the most famous, or at least the most studied, clean surface phase transition is one that occurs on Si(0 0 1) [46–52]. Since 1978 there have been over 4000 papers published about this surface, in large part due to its technological importance. At room temperature the surface reconstructs to eliminate the unbonded electrons created by breaking the Si–Si bonds to form a surface. The reconstructed surface consists of rows of dimers as shown in Fig 10(b), but when the surface is cooled to ~100 K a new structure appears which is composed of asymmetric dimers (called buckled dimers) as shown in Fig. 10(a) [50]. An electron diffraction study found that the phase transition took place over a fairly broad temperature range and was consequently labeled a second order, order–disorder transition. The buckled dimer configuration shown in Fig. 10(a) melts into the symmetric arrangement as the temperature increases. A second order phase transition is one in which the order parameter that characterizes the existence of one phase changes continuously with temperature. This seemed to be a solved problem, with the ground state being the buckled dimer, which underwent an order–disorder transition with increasing temperature. Ab initio theory confirmed that the buckled dimer was indeed the ground state.

> *Truth is eternal—until a new truth replaces it*
> Morton F. Spears, "Capacitance Theory of Gravity"—1991

There was a warning issued in 1994 that a small number of defects could dramatically change the nature of this phase transition. On the eve of the new millennium this consistent textbook story on the surface structure of clean Si(0 0 1) was turned on its head. Low-temperature STM (down to 5 K) revealed that the true ground state of this surface is a symmetric dimer, leading to speculation that antiferromagnetic ordering was involved in the ground state [51,52]. This provides an important lesson to all surface physicists—lower the temperature!

The STM is a magnificent tool to study what the atoms are doing in real space as a phase transition occurs, especially in one or two dimensions.

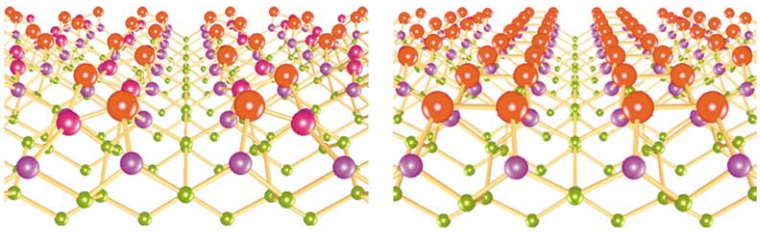

Fig. 10. Stick and ball model of the two reconstructed surface structures seen on the reconstructed surface of Si(0 0 1). When a Si(0 0 1) surface is created by cutting the solid into two pieces each exposed Si atom has lost two out of four of its nearest neighbors, leaving these surface atoms with two broken (dangling) bonds. The surface reconstructs to eliminate as many dangling bonds as possible. On this surface the reconstruction results in rows of dimers as indicated by the red atoms in (b). If the red atoms were removed in this figure the purple Si atoms would be in the positions dictated by the bulk structure. At room temperature the dimer rows are symmetric (b) but when the temperature is lowered to ~100 K a transition occurs to an asymmetric or buckled configuration shown in (a). In each dimer the bright red atom is up and the dark red atom down with adjacent dimer pairs in a row or across rows being out of phase. Recent STM measurements at ~5 K have shown that the true ground state is the symmetric dimer configuration shown in (b) [51,52] (courtesy of T. Uda and K. Terakura).

Here we show that an STM study of the role of defects in a 2D phase transition can change the way scientists think about this subject, i.e. a paradigm shift. It is generally recognized that defects can play a critical role in phase transitions, especially in reduced dimensionality [43]. Mobile defects and the onset of their spatial long-range ordering are often invoked as a microscopic explanation of some experimental observations in low-temperature phase transitions [53–55]. For example, Mutka, in his article on the influence of defects and impurities on charge density waves (CDWs) comments [53]:

> *Defects in CDW compounds are inevitable, and their influence on the CDW phenomena is more a rule than an exception—The strong connection to defects influences the whole physics of CDWs with consequences that are manifest in a wide space and time scale from microscopic to macroscopic... This is the reason why microstructural characterization of the CDW is of primary importance...*

A CDW is an electronic perturbation of a solid that lowers the total energy by the formation of an electron CDW with a different periodicity than the solid [56,57], i.e. broken symmetry. A CDW is usually accompanied by a small lattice distortion. Mutka speculates on the possibility of metastable defect configurations and to the concept of defect-density waves (DDW) [53]. Baldae has hypothesized that a modulation of the occupation probability of defects along the 1D lattice occurs in potassium cyano-platinide [55]. Even though the alignment of defects has not been directly demonstrated experimentally, the concept has proven to be a useful microscopic description for a variety of experimental data [53–55].

Before discussing the STM measurements of defect mediated 2D phase transitions the system being investigated needs to be introduced. Fig. 11(a) shows a marble model of what is referred to as the α phase of Sn on Ge(1 1 1) [58]. The Sn atoms (light blue) are positioned on top of three Ge atoms (purple with red bonds) in the first layer of the (1 1 1) surface. The red lines show the basic building block (called unit cell) for the room temperature structure labeled $\sqrt{3} \times \sqrt{3}$ and the low-temperature CDW structure labeled (3×3). The important observation is that in the room temperature phase there is only one Sn atom in a unit cell, which means that every Sn atom is identical. But in the CDW phase there are three Sn atoms in each unit building block. In Fig. 11(b) are the original STM images [58] showing the changes that are observed when the temperature is lowered. The RT STM images shown at the top (small inserts) exhibit the same symmetry in the filled and empty state images, indicating that the STM image is reproducing the geometric structure shown in Fig. 11(a). When the temperature is lowered the images are complimentary. The empty state image has two out of the three Sn atoms in the (3×3) unit cell bright forming a honeycomb structure. In the filled state image, the other atom in the unit cell is bright forming a hexagonal lattice. This complimentarity is the signature of a charge density wave. A simple interpretation is that two atoms in the unit cell are positively charged ($+q/2$ seen in empty state images) and one negatively charged ($-q$ seen in the filled state image). There is a lattice distortion accompanying the CDW, one Sn atom in the unit cell moves up and the other two move down ($\sim$0.3 Å vertical buckling). One can take three waves (120° apart) with the wavelength associated with the (3×3) structure in Fig. 11(a), sum their amplitude and square (charge density) to reproduce the images of the CDW phase.

The red arrows in Fig. 11 indicate the positions of Ge substitutional defects, i.e. Ge atoms from the substrate that have taken the place on an Sn atom in the thin film. These defects control the nature of this phase transition. As we subsequently show, there are two inextricable intertwined phase transitions—a first-order transition involving the alignment of the defects and a second-order CDW condensation. A clarification of the definition of first- and second-order phase transitions is presented later.

The ground state of this system is the (3×3) CDW structure, but at temperatures above the transition temperature Ge substitutional defects stabilize damped CDW-like waves in their vicinity. Experimentally it was realized that these damped

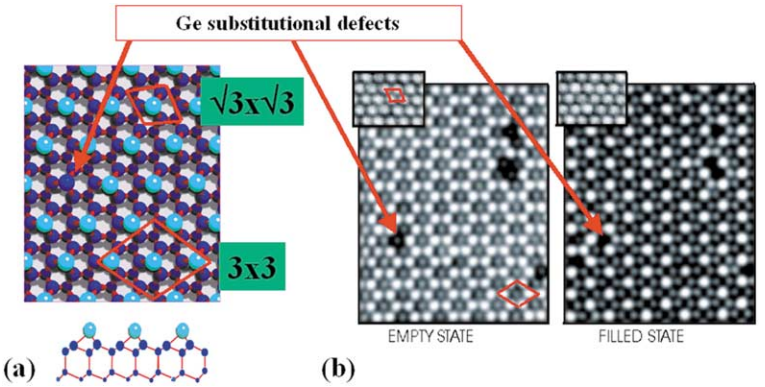

Fig. 11. Structural model and STM images of the symmetry lowering phase transition, from $(\sqrt{3}\times\sqrt{3})R30°$ to (3×3) structure observed in a thin metallic film of Sn on Ge(1 1 1). (a) A marble model of the room temperature structure of this system, where the Sn atoms are shown as light blue balls and Ge atoms are indicated as dark blue. The drawing at the bottom shows a side view of the surface. At room temperature, the Sn atoms form a structure with respect to the bulk truncated Ge structure denoted by $(\sqrt{3}\times\sqrt{3})R30°$. This notation means that the unit cell or basic building block of this structure (shown in red at the top) contains one Sn atom and three surface Ge atoms. When the temperature is lowered there is a transition to a new structure with a 3×3 unit cell shown at the bottom right of (a). The new unit cell triples in size compared to the $\sqrt{3}\times\sqrt{3}$ unit cell and now contains three inequivalent Sn atoms. (b) The STM observations above and below the phase transition temperature are shown in these two sets of images, labeled 'empty' and 'filled' state, which corresponds to the voltage bias between the sample and the STM tip. In 'filled' state images the tip is positive with respect to the sample and electrons tunnel from occupied states (filled) in the sample to the tip. In 'empty' state images the voltage on the tip is negative and electrons tunnel from the tip into unoccupied (empty) states in the sample. The two small images in the upper left hand corners are the room temperature images, and the big STM images are at low-temperature. The Sn atoms appear equivalent in both filled and empty state STM images taken at room temperature. At low temperature there are two bright and one dark atoms per unit cell (seen unit cell in empty state image) observed in the empty state image, thus indicating lowering of the symmetry. The filled state image has one bright and two dark Sn atoms in each unit cell. The complimentarity of the filled and empty state images at low-temperature is a signature of the CDW formation. Arrows in (a) and (b) mark the position of Ge substitutional defects that affects the CDW formation [58].

CDWs were temperature dependent and could be fitted with a simple exponential function $\exp[-|\mathbf{r}-\mathbf{r}_n|/l(T)]$, where $l(T)$ is the decay length of the CDW away from the defect located at $\mathbf{r}_n$ [59,60]. Fig. 12(a) shows a simulation of the damped CDW, stabilized by a single Ge substitutional defect. The defect creates a honeycomb local disturbance (in a filled state STM image). As the temperature decreases, the range of the stabilized CDW extends, shown in the simulation in Fig. 12(b) which illustrates the interference in the stabilized CDWs from two defects. The interference produces the hexagonal lattice seen in the STM filled state images (Fig. 11(b)). This is the first direct indication that defects are important in the creation of the CDW [59]. A single defect would create a honeycomb lattice seen in the filled state STM images, while multiple defects create a hexagonal lattice.

Many STM images were fitted with the simulations depicted in Fig. 12. The positions of the defects in the real image were transferred to the simulation and the magnitude of $l(T)$ adjusted until interference patterns in the experimental and theoretical images agreed. Fig. 13(a) shows the measured inverse decay length $1/l(T)$ as a function of temperature for Sn/Ge(1 1 1) [59]. The length parameter diverges at $T_1 = 70$ K, leading to the prediction that the CDW phase transition from a single defect would occur at this temperature T_1 Fig. 13(b) shows the (3×3) diffraction intensity calculated from the simulated images, or measured with low energy electron diffraction (LEED) [61] as a function of temperature. This is an appropriate order parameter for this phase transition. An order parameter is used to distinguish one phase from the other. It is by definition zero in the high-temperature phase, and saturates in the

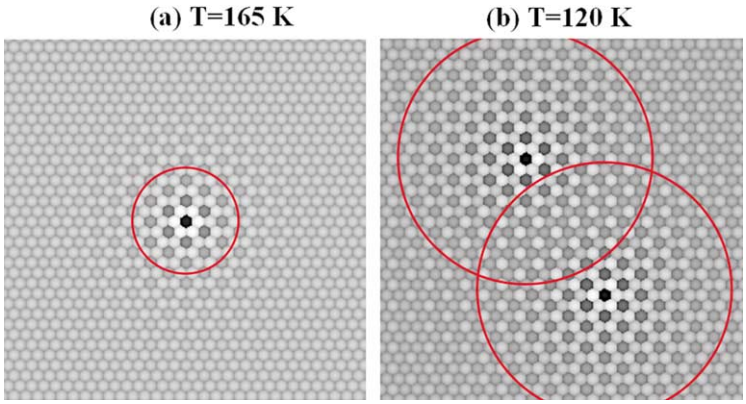

Fig. 12. Simulation of a defect-induced CDW. A defect can produce a periodic oscillation of charge in its vicinity. The extent of these damped density oscillations depends upon the temperature, increasing in range as the temperature is lowered. The simulated STM image for a single Ge defect (a) shows damped CDWs at a temperature equivalent of $T = 160$ K. The characteristic decay length of this wave is shown by the red circle and is $l = 25$ Å. When there is more than one defect present, the resultant charge perturbation is a complex interference pattern. The simulation (b) is a result of interference of waves from two defects at a temperature $T = 120$ K, with a decay length shown by the red circles of $l = 50$ Å [59].

low-temperature phase. Since this order parameter is continuous, this is a second-order phase transition.

There is another transition that occurs in this system. At a temperature $T_2 < 120$ K the decay length is longer than the average defect–defect spacing l_{av} indicated in Fig. 13(a). The (3×3) unit cell in Fig. 11(a) shows that there are three Sn atoms in each cell. This means that there are three possible CDW domains depending on which of the three atoms is negatively charged. Since Ge substitutional atoms do not like to sit on a charge maximum site, a random distribution of Ge defects would have, on average, 1/3 on unfavorable sites. A careful statistical counting of the defects in the STM images has proven that they move as the temperature is lowered [59,60]. The measured result is shown in Fig. 13(c), indicating an abrupt alignment of the defects at ~120 K. Fig. 13(d) shows the results of a Monte Carlo simulation of the defect alignment P_C. P_C is the order parameter for the defect alignment phase transition.

There are two defect density dependent interlocked phase transitions in this system. A second-order CDW transition characterized by the order parameter of the (3×3) diffraction intensity in Fig. 1(b) and a first-order DDW characterized by the defect alignment probability function P_C (Fig. 13(d)). A phase transition is first order if the order parameter is discontinuous. Both transitions depend intimately upon the defect density.

Undoubtedly, this is just the beginning of STM studies of defect mediated phase transitions in one and two dimensions. We can look forward to STM images of DDWs, and new microscopic theories of defect-mediated phase transitions in reduced dimensionality. When there are only a few "wrong" atoms we talk about defects. Understanding the interaction of defects with the host system and with each other is the first step to a microscopic picture of binary systems. On a more global scale the real space images obtained with the STM compliment more established diffraction experiments (momentum space), and contribute a new perspective to the understanding of collective phenomenon in complex–inhomogeneous materials.

The example given here of defect alignment falls in the family of what is now called self-assembly, or self-organization. Self-assembly refers to systems that, under the correct conditions, will organize themselves into a desirable state. Often the final structures are periodic on the nanoscale and consequently are of special importance to the emerging field of nanotechnology.

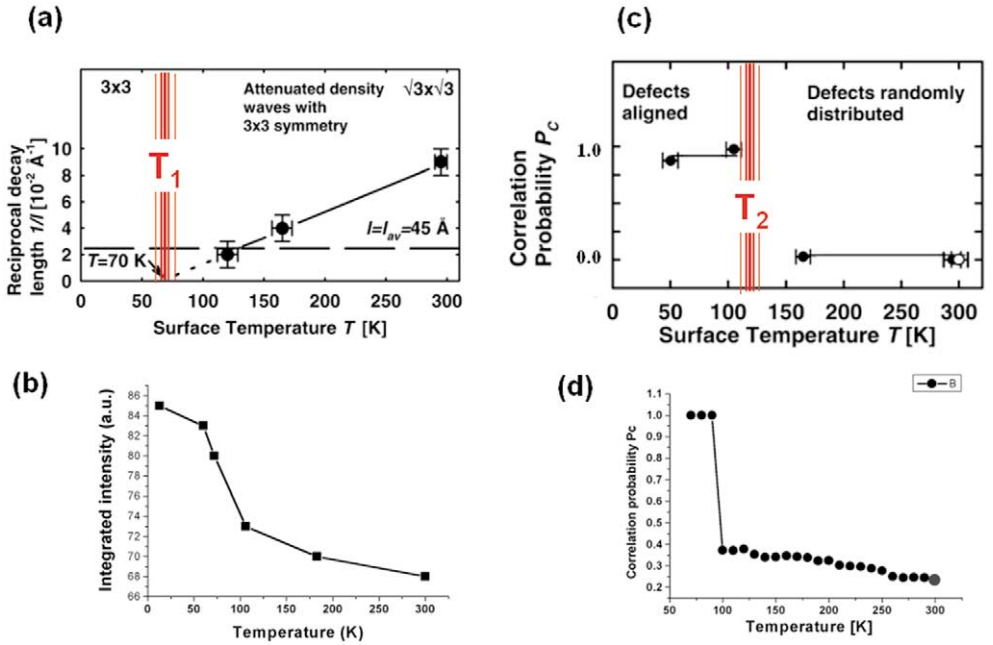

Fig. 13. Representation of the two intertwined phase transitions associated with the system described in Fig. 11, 1/3 of a monolayer of Sn on Ge(1 1 1). (a) The measured temperature dependence of the inverse decay length, $1/l(T)$, of the CDWs induced by substitutional Ge defects in Sn overlayer. Extrapolation can be used to determine the temperature at which the CDW transition would occur in the absence of defects (T_1). The horizontal line marked by l_{av} denotes the average spacing between Ge defects in the Sn overlayer. The order parameter of CDW transition, integrated intensity of (3×3) spot, is shown in (b). In the defect populated system it never becomes zero. Due to the CDW-mediated defect–defect interaction a CDW transition shown in (a) and (b) is accompanied by defect-ordering transition. A probability function P_C is defined as 0 if there is an equal distribution of Ge substitutional atoms on all three possible CDW lattices and is equal one if the Ge atoms in a single CDW domain are all located on the two lattices with charge minimum. The measured order parameter of defect alignment, the correlation probability P_C vs. temperature is shown in (c), indicating an abrupt transition at a temperature T_2. (d) The defect alignment has been simulated using a simple electrostatic model for the interaction of a defect with all of the defect-induced CDWs in the system. The simulated order parameter P_C for the defect alignment transition is shown in (d) [59–61].

3.3. The surfaces of complex highly correlated materials

In this section we illustrate how surface science techniques, both experimental and theoretical, are ideal for uncovering the fascinating physics taking place at the surfaces of highly correlated materials such as TMOs. Three examples will be given. (1) A study of electronic nanophase separation in the CMR materials [62], as discussed in Section 1; (2) the discovery of microscopic spatial electronic inhomogeneity in the superconducting gap in a high-T_c sample [63], and; (3) the identification of surface stabilized structural and magnetic phases in a spin triplet paired TMO superconductor [64].

The phenomenon of electronic nanophase separation is at the heart of the basic physics of CMR materials. In 1999 Fäth et al. used a variable temperature STM equipped with a high magnetic field to study the spatial electronic properties of the CMR materials $La_{0.7}Ca_{0.3}MnO_3$ [62]. Fig. 5(a) displays the coupled metal–insulator (M–I)—ferro–paramagnetic transition in the same material but with a slightly higher doping level, $x = 0.35$. The transition temperature is ~240 K when there is no applied magnetic field and it decreases with increasing magnetic field. Fig. 14 shows a series of spatial images (STM) of this material at a temperature slightly below the zero field transition temperature (Fig. 5(a)) as a

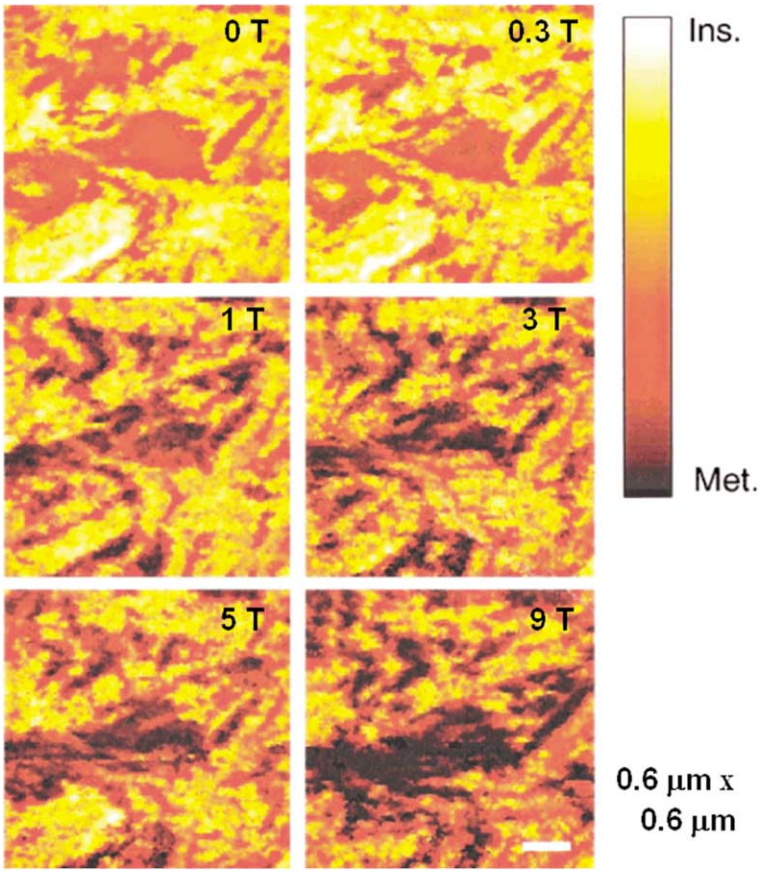

Fig. 14. STM spectroscopic images (0.61×0.61 μm^2) from the surface of $La_{0.7}Ca_{0.3}MnO_3$ taken just below the M–I transition temperature T_c (240 K), showing the evolution of local electronic structure under the influence of an external magnetic field [61]. The phrase spectroscopic image refers to the measurement procedure, where images were taken by measuring the spatial differential conductance dI/dV (I is the tunneling current and V the applied voltage) at a bias voltage of 3 V. The authors have demonstrated that spectroscopic images at this bias voltage are sensitive to the local metallic behavior. The bar on the right indicates the insulating vs. metal character. The magnetic field is increased from zero to 9 T. It is found that microscopic electronic inhomogeneities appear in this material and that applying a magnetic field enhances the size of the metallic domains until they are interconnected, i.e., a percolation behavior.

function of applied magnetic field. The authors have shown that the differential conductance dI/dV (I is the tunneling current and V the applied voltage) at a voltage of 3 V can be used as a direct measure of the metallic character. The dark regions in the images are metallic. It is easy to see that there are electronic inhomogeneities on the 20 nm to several 100 nm scale, with the coexistence of insulating, metallic, and intermediate regions. The observed nanophase separation is not as well behaved as is predicted theoretically and shown in Fig. 6. As the magnetic field is increased the dark regions (metallic) grow at the expense of the light (insulating) regions. When metallic regions (dark colour) connect on a macroscopic scale the sample becomes a metal. This phenomenon is called percolation.

The STM is an excellent tool for monitoring the surfaces of these spatially inhomogeneous systems as they approach the phase transition temperature or the percolation threshold. It is likely that surface scientists, working in this field over the next

decade, will be among the first to understand the processes that drive and control the exotic properties of these materials. There is a tremendous opportunity for a surface scientist who knows how to prepare, modify, and carefully characterize the surfaces or interfaces of these TMOs.

The second example is an exciting measurement of the spatial inhomogenieties in the superconducting gap for $Bi_2Sr_2CaCu_2O_{8+x}$ created by the broken symmetry associated with the excess O doping (x) in these samples [63]. In a conventional metal, excess doping might be expected to create local inhomogeneities in the structure but the electronic structure usually remains homogeneous due to the short-range screening in metals. As will be shown in this example, this is apparently not the case for the high-T_c superconductor $Bi_2Sr_2CaCu_2O_{8+x}$. The structure of this material and its cleavage plane (BiO) are shown in Fig. 15.

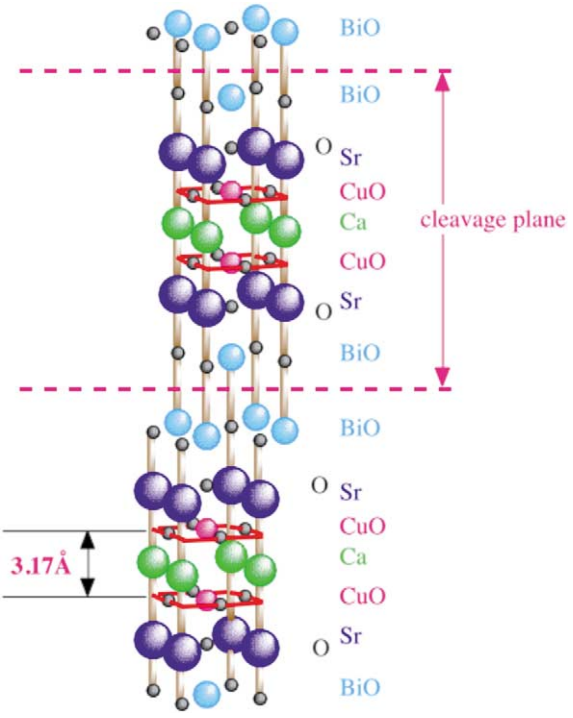

Fig. 15. Structural model of $Bi_2Sr_2CaCu_2O_{8-x}$. The cleavage plane is marked by the arrow and the color code of the atoms is indicated. Notice that the CuO superconducting plane is the third plane from the surface which is the BiO plane.

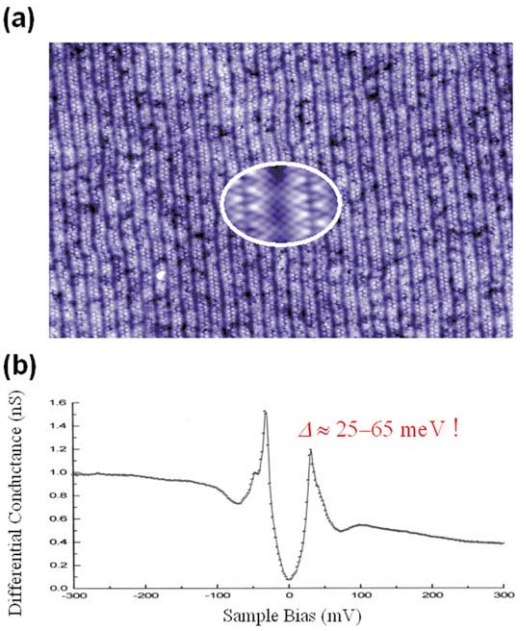

Fig. 16. (a) STM constant-current image at 4.2 K of $Bi_2Sr_2CaCu_2O_{8-x}$ taken at a tunneling current of 100 pA and a voltage of 100 mV [62]. The size of the picture is 80×125 nm^2. The center inset is a zoom-in image (5×) showing the detailed lattice structure on the surface. (b) The differential conductance (dI/dV) vs. sample bias, showing the electronic density of states including the superconducting energy gap of the local position of the sample. The sharp peaks around zero bias are associated the "quasiparticle" density of states and superconducting energy gap (Δ).

Superconductivity occurs in the CuO planes which are the third and fifth planes below the surface. The optimized superconducting transition temperature is ~90 K for a doping level of $x \sim 0.16$. Fig. 16(a) shows a high-resolution constant current topograpic image of the surface showing the structure of the BiO plane. The center insert is an enlargement by a factor of five. Fig. 16(b) is a differential conductance (dI/dV) plot for a specific region on the sample. These tunnel junctions (tip to sample) are not ohmic so the resistance and the conductance are a function of voltage. A conductance plot of $I(V)/V$ is not a straight line and differential conductance dI/dV plot-like that in Fig. 16(b) displays structure related to the electronic properties of the local position on the sample. The sharp structure around zero bias voltage

is associated with the superconducting gap Δ, while the signal at much larger bias voltages is related to the local density of states at the surface [63].

These authors found that the magnitude of the superconducting gap as well as the local density of states were dependent on the position of the tip on the surface, i.e. spatial electronic inhomogeneity. In a *tour de force*, Pan was able to map out the spatial distribution of the magnitude of the superconducting gap, which is shown in Fig. 17(a) [63]. The spatial inhomogeneities are a few nanometers in extent. Fig. 17(b) shows a histogram of the observed superconducting gap size, showing an average value of 40 meV, the value usually observed in macroscopic measurements. But there is a variation of ~40 meV in the gap size depending on the position of the STM tip. There is a spatial correlation between the local density of states and the superconducting gap. The higher the local density of states the smaller the superconducting gap. Both exhibit Gaussian-like distributions, with a short autocorrelation length of ~14 Å. This length scale is surprising because the in-plane superconducting coherence length is believed to be ~25 Å [63].

The origin of the length scale of the electronic inhomogeneities in the density of states and the superconducting gap seems to be directly related to the density of excess oxygen x. For optimal

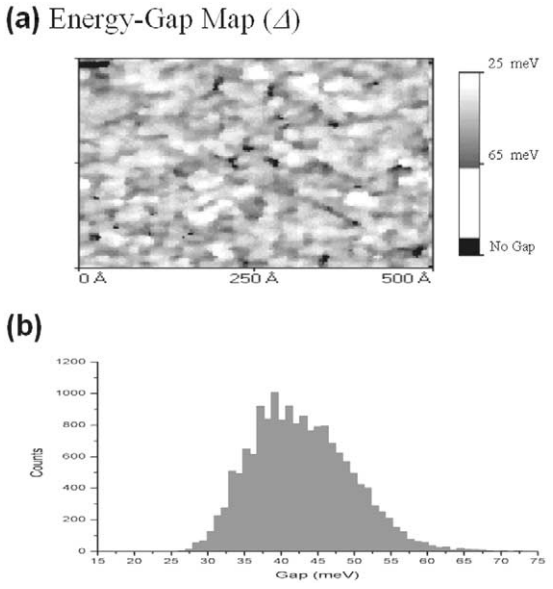

Fig. 17. (a) The spatial distribution map of the measured superconducting energy gap Δ from the surface of $Bi_2Sr_2CaCu_2O_{8-x}$ at 4.2 K, revealing the spatial electronic inhomogeneity on nanometer-length scale. (b) A histogram of the spatial distribution of gap sizes [63] showing a large spatial variation of the gap with a average value of ~40 meV which is usually observed in macroscopic.

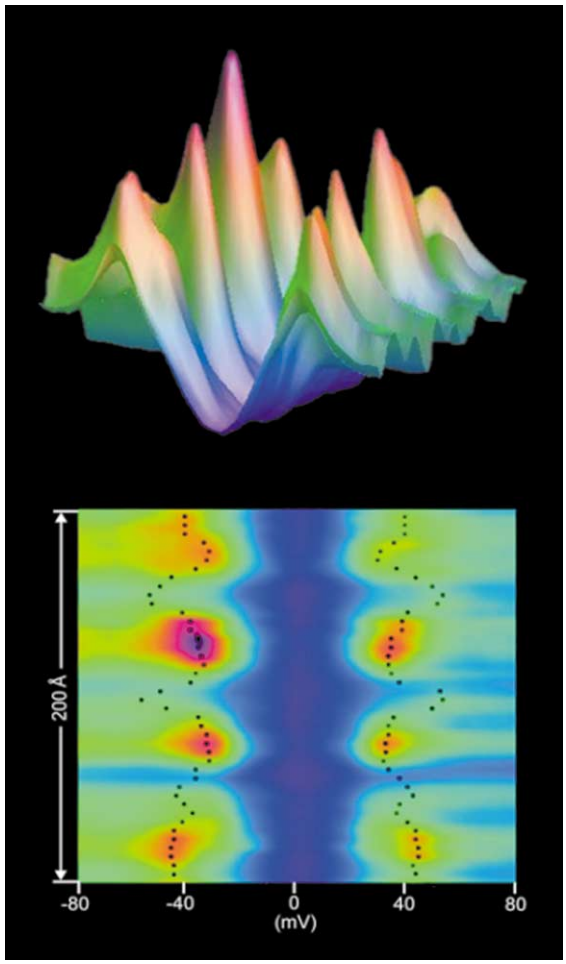

Fig. 18. 2D (bottom) and 3D (top) plots of the spatial dependence of the differential conductance showing the microscopic inhomogeneity in the magnitude of the superconducting gap in $Bi_2Sr_2CaCu_2O_{8-x}$ [63]. The dots in the bottom panel trace out the superconducting band edges.

doping of $x = 0.16$ the average inter-dopant spacing is ~13.5 Å. Fig. 18 is a 2D and 3D drawing of the spatial dependence of the differential conductance in this sample. The speculation is that the local density of states away from the gap is believed to be a good measure of the oxygen concentration [46]. When the STM tip is close to an oxygen atom (dopant) the density of states at high bias voltages is low and the superconducting gap is large, as displayed in Fig. 18.

This study of the spatially dependent electronic properties of a high-T_c superconductor raises many questions and suggests many new experiments. What creates the inhomogeneous superconducting gap? Is it the broken symmetry created by the excess doping of oxygen x? Is this a general property of all high-T_c materials? If so, is this a general and fundamental property of high-T_c superconductors? Is this the first picture of inhomogeneity-induced superconductivity [37]? Will these and future measurements lead to a deeper understanding of high-T_c superconductivity? Is this a surface affect? Is the oxygen concentration at the surface the same as in the bulk? Again, we stress that here is a tremendous opportunity for a surface physicist to have an impact on an important area of CMP.

The last example illustrates the stabilization at the surface of low energy excited states (structural and magnetic) in the bulk of the unconventional superconductor Sr_2RuO_4 [64–67]. Sr_2RuO_4 is the only known layered perovskite without copper that exhibits superconductivity ($T_c \sim 1.5$ K) [65]. It is also a superconductor without additional oxygen doping. It has attracted much attention because it shows so-called spin-triplet pairing symmetry with a p-wave order parameter [66,67]. The pairing symmetry is determined by total spin (spin singlet or triplet) and angular momentum channels (s-wave, p-wave, and so forth) characterizing the Cooper pairs. Pairs of fermions must have antisymmetric wave functions under particle interchange. For a Cooper pair, this requirement implies a relationship between the orbital and spin character. Orbital wave functions with even values of the orbital quantum number ($l = 0, 2, \ldots$) are even under particle interchange and therefore require odd symmetry in the spin wave function, i.e. spin singlets with one spin up and one down. High-T_c cuprates, which are antiferromagnets rendered superconducting by doping, are now known to have spin-singlet pairing in a d-wave ($l = 2$) orbital channel. In Sr_2RuO_4, experiment and theory suggests that the orbital wave function in the Cooper pair has p-character ($l = 1$) such that the spin wave function is required to be triplet (spins aligned). Obviously, spin-triplet pairing favors ferromagnetic spin fluctuation in contrast to that in cuprates where the spin-singlet pairing is associated with antiferromagnetic fluctuation.

The bulk of Sr_2RuO_4 has the RP structure for $n = 1$ shown in Fig. 4, with a nonmagnetic ground state. However, this ground state is close to structural and magnetic instabilities. A common characteristic of this class of materials, is that the energy difference between different structural/magnetic phases is very small. Creating a surface by cleaving a single crystal is a controlled way to disturb the coupled system by breaking the symmetry without changing the stoichiometry. With this example we illustrate that this unique environment at the surface could produce new phenomena, while providing a fresh approach to the study of the spin-charge-lattice coupling in these complex materials.

Fig. 19(b) shows a large scale STM image of a surface cleaved inside a vacuum system and transferred to an STM stage [64]. There are large flat terraces with an extension up to 10 μm. All step heights are integral multiples of half the unit cell (6.4 Å) shown in Fig. 19(a). Experimental electron diffraction determinations of the surface structure and ab initio calculations prove that the surface is the SrO plane, as expected from looking at Fig. 4 ($n = 1$). The enlarged STM image, with atomic resolution, shown in Fig. 19(c) as well as LEED patterns shown in Fig. 20(a) indicate that the surface is not bulk truncated but reconstructed. As in Fig. 11 for Sn/Ge(1 1 1), we have drawn in the basic 2D structure (unit cell) in Fig. 19(c). The reduction in symmetry at the surface caused by the reconstruction creates fractional order diffraction spots in the LEED pattern shown in Fig. 20(a), marked by the white arrows. The measured and calculated surface structure

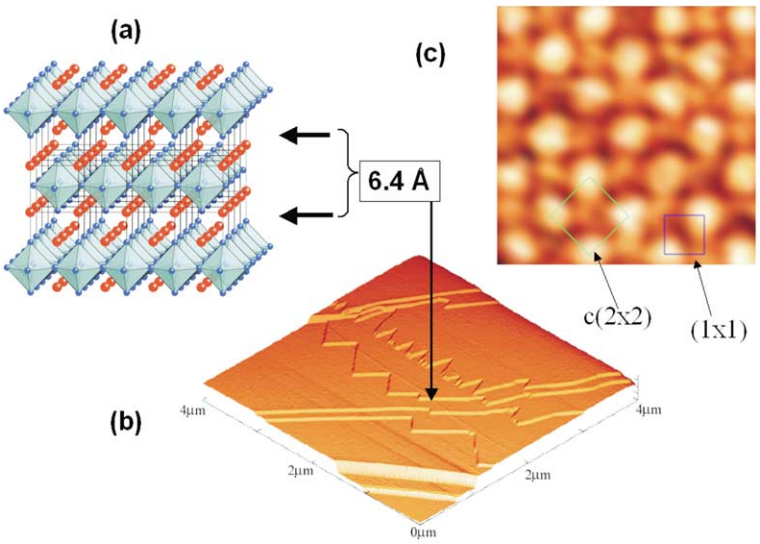

Fig. 19. (a) Structural model of Sr_2RuO_4 (red: strontium, blue: oxygen, green: ruthenium in the center of the octahedron). The dark arrow indicate the cleavage planes and the spacing between these planes. (b) STM image of a 4×4 μm^2 surface area (room temperature with +0.5 bias voltage) showing extremely large terraces and steps. (c) Atomically resolved STM image of 26×12 Å^2 containing 7×7 strontium sites. Theoretical calculation of the local density of states showed that the bright spots correspond to the strontium site ($T = 300$ K, sample bias voltage −0.75 V). The bulk (1×1) (blue) and surface c(2×2) reconstructed unit cell (green) are indicated [64].

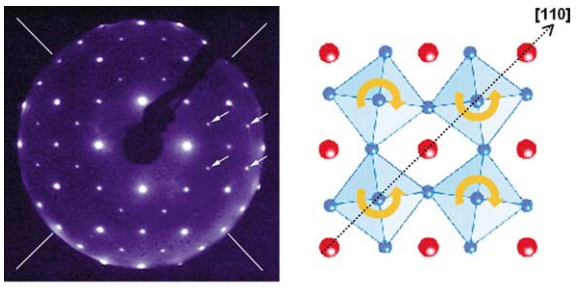

Fig. 20. (a) LEED pattern showing fractional spots (marked by arrows) created to the surface reconstruction. There are missing fractional order spots in the LEED pattern (indicated by white lines) that are important in determining the symmetry of surface structure [64]. Electron energy $E = 195$ eV, temperature $T = 80$ K. (b) Ball model of the surface structure with rotated octahedra (top view). The direction of the rotation is shown by the yellow arrows. The direction of propagation of the soft-bulk phonon is phonon mode is in the diagonal direction [1 1 0].

is shown in Fig. 20(b). The octahedra in the surface plane are rotated alternating clock- and anticlockwise around the surface normal direction. This rotation is exactly the low energy vibrational (phonon) mode in the bulk, so the surface has stabilized a geometric instability present in the bulk.

Experimentally, the octahedra rotation is $9 \pm 3°$. First-principles calculations of the ground state surface structure confirm the octahedra rotation. The optimized structure for a nonmagnetic surface is a surface layer with octahedra rotated by 6.5°. This reconstruction is driven by compressive strain in the RuO_2 layers. According to theory, the reconstruction enhances ferromagnetic ordering, which in turn stabilizes the distortion further and increases the rotation angle to 9°. The ground state of the surface is, according to theory, ferromagnetically ordered, driven by the structural distortion of a rotation of the octahedra. It is worth mentioning that there is a ferromagnetic fluction in the bulk. Broken symmetry at the surface stabilizes not only the lattice but also a magnetic structural instability that existed in the bulk.

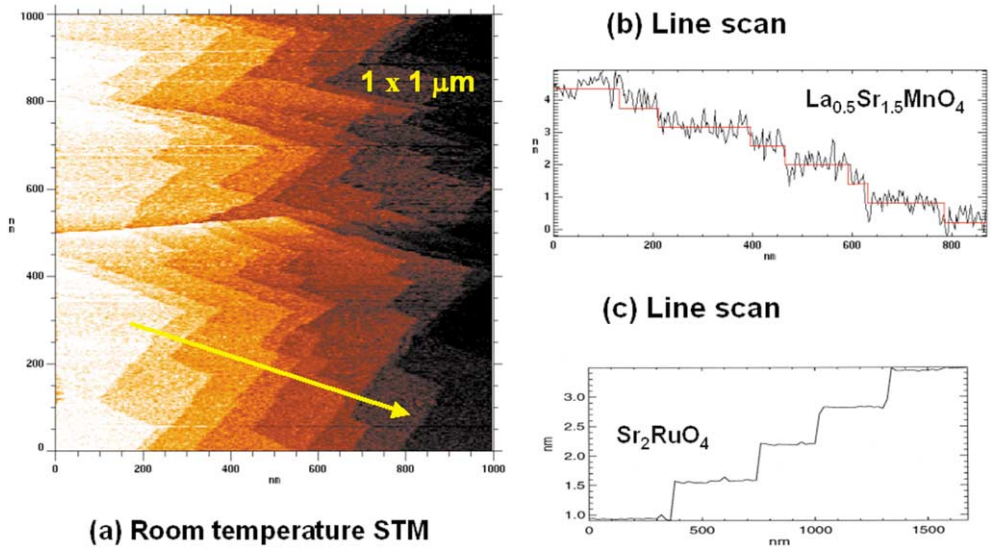

Fig. 21. (a) Large area STM image of $La_{0.5}Sr_{1.5}MnO_4$ cleaved in the vacuum and imaged at room temperature with a bias voltage of 2.5 V. (b) STM constant current height scan along the yellow line shown in (a). (c) Line scan for a freshly cleaved sample of Sr_2RuO_4 like the one shown in Fig. 18. Though both materials have the same bulk structure, the surface roughness is drastically different, caused by the electronic nanophase inhomogeneities occurring in $La_{0.5}Sr_{1.5}MnO_4$ but not in Sr_2RuO_4.

This investigation of the surface of Sr_2RuO_4 illustrates that existing surface structural and electronic probes can be used on these complex materials. It opens up many exciting prospects, relevant to the bulk and surface properties of layered TMOs. For example, there is the possibility of the coexistence of FM and superconductivity in layered superconductors [68] or at the surface of high-T_c materials [69]. The challenge for the surface physicist is to develop techniques capable of structural, magnetic and electronic measurements on that same surface, or ideally at the same place on the surface as a function of temperature and magnetic field.

3.4. Nano-scale patterning of the surface of complex transition-metal oxides

The final example of this paper illustrates the possibility of utilizing the close coupling of the spin, charge, and lattice degrees of freedom in complex TMOs to artificially pattern the surface on a nanoscale. The hint that this might work was presented in Fig. 5(c) where it was shown that a light beam could convert an antiferromagnetic-ordered insulating phase of a TMO into a ferromagnetic-ordered metallic phase. If you can accomplish this switching with a laser beam then you should be able to achieve the same conversion with the current from an STM tip.

We have investigated the layered manganite $La_{0.5}Sr_{1.5}MnO_4$ which has the same basic crystal structure as Sr_2RuO_4 ($n = 1$ in Fig. 4). In contrast to Strontium Ruthenate, this material is a charge-ordered insulator with a charge ordering transition at 220 K and it is antiferromagnetically ordered below 110 K [70]. Fig. 21(a) shows a large scale STM image of a cleaved sample of this material at room temperature. It is easy to see the step edges and terraces as in the equivalent image for Sr_2RuO_4 displayed in Fig. 19. The striking difference is that the material is electronically very rough. A line scan across the sample (yellow line in (a)) is shown in (b) where you can see that the modulations are almost as big as the step height. This is caused by electronic nanophase separation in this material, similar to what was shown for $La_{0.7}Ca_{0.3}MnO_3$ in Fig. 14, except that in this case

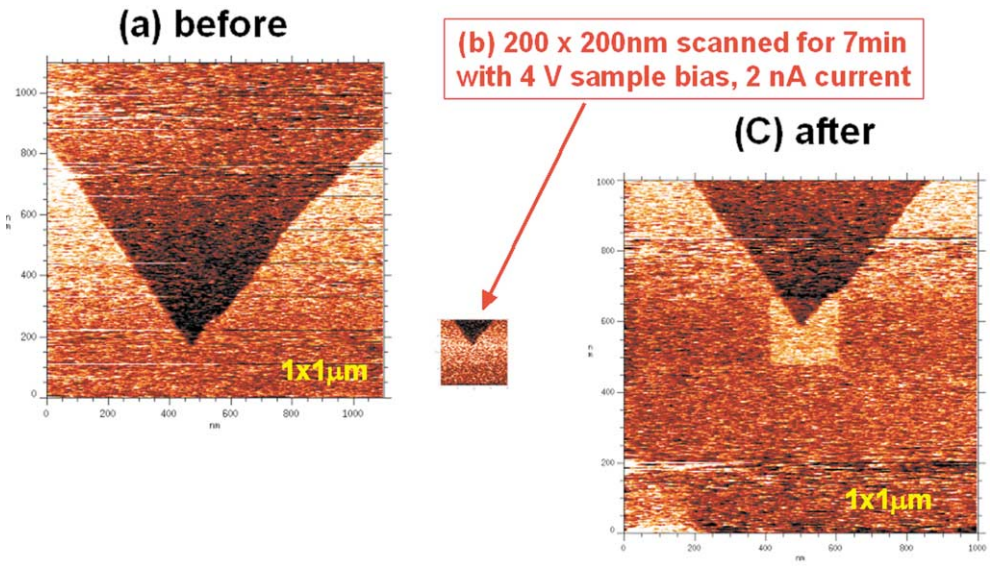

Fig. 22. Panel (a): STM image of a 1100×1100 nm^2 area of $La_{0.5}Sr_{1.5}MnO_4$ vacuum cleaved surface scanned at room temperature with +2.5 V bias voltage. The triangular structure is the image of the step. (b) After taking the image (a), a 200×200 nm^2 square area centered around the step-corner was scanned for 7 min with 4.0 V bias voltage. (c) 1000×1000 nm^2 area centered around the same step corner imaged after the procedure described above in (b). The excessively scanned area of 200×200 nm^2 looks brighter than the rest of the terraces, indicating a better conductivity of the surface after scanning for some minutes with elevated bias voltage.

the length scale associated with the nanophases is much smaller, ~20 nm. For comparison, Fig. 21(c) shows a similar line scan of Sr_2RuO_4, where the roughness is caused only by the atomic corrugation.

Fig. 22 illustrates what happens if the tunneling current density is increased dramatically. You write! Panel (a) is a large area scan with a bias voltage of 2.5 V. After this scan was taken, a smaller area (200×200 nm) was scanned with an increased voltage of 4 V at 2 nA current for approximately 7 min. Fig. 22(c) displays a subsequent broad area scan showing that the area scanned in (b) is much brighter, indicating that it is more metallic. It seems possible to write on this surface creating nanoscale ferromagnetic-ordered metal patches! Generally speaking, it should be possible to destroy the bulk charge ordered state (insulating and antiferromagnetic-ordered states) at the surface, creating a ferromagnetic-ordered metal. There is no obvious reason why this conversion cannot be patterned with an electron or photon beam.

4. Conclusion

What an exciting prospect: Surface scientists can change the way the materials community thinks. All we have to do is *engage*.

Many a false Step is Made by Standing Still—Chinese fortune cookie

You miss all of the shots you don't take—Wayne Gretzky

If the surface physics community engages in contemporary materials physics, we can look forward to many decades of exciting discoveries. The sky is the limit, or perhaps more appropriately, the cosmos is the limit. All physicists search for universality that is the ability to map their observations or theories onto a wide variety of problems of very different length scales. Fig. 23 shows that the STM images of the electronic inhomogeneities at the surface of $La_{0.5}Sr_{1.5}MnO_4$ (top right) map onto spatial inhomogeneities seen in UV emission

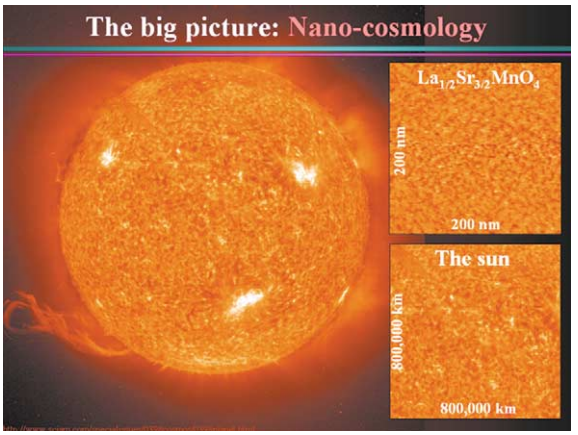

Fig. 23. Nanocosmology, comparing the electronic spatial variation for $La_{0.5}Sr_{1.5}MnO_4$ with the spatial variation in UV emission from the surface of the sun. There are 15 orders of magnitude difference in the length scales. The sun image is a courtesy of SOHO/EIT consortium. SOHO is a project of international cooperation between ESA and NASA.

image of the surface of the sun. This is true universality, since the difference in length scale is ~15 orders of magnitude. We are truly living in the world of nano-cosmology. Our contribution has come full circle, back to the introduction, where we introduced Broglia's article in this special issue of Surface Science titled "The surface of compact systems: from nuclei to stars".

References

[1] Nanotechnology: Shaping the World Atom by Atom, National Science and Technology Council, Committee on Technology, 1999 http://www.nano.gov/press.htm.
[2] D.H. Lowndes (Ed.), Nanoscale Science, Engineering and Technology Research Directions. Basic Energy Sciences Program, US Department of Energy, ORNL, 1999.
[3] R.A. Broglia, The surfaces of compact systems: from nuclei to stars, Surf. Sci. 500 (2002) 759.
[4] J.M. Greenberg, Cosmic dust and our origins, Surf. Sci. 500 (2002) 793.
[5] D.A. Williams, E. Herbst, It's a dusty Universe: surface science in space, Surf. Sci. 500 (2002) 823.
[6] T.E. Madey, R.E. Johnson, T.M. Orlando, Far-out surface science: radiation-induced surface processes in the solar system, Surf. Sci. 500 (2002) 838.
[7] Complex Systems: Science for the 21st Century, Office of Science Workshop, US Department of Energy, March 5–6, 1999, available at http://www.er.doe.gov/production/bes/complexsystems.htm.
[8] Condensed-Matter and Materials Physics: Basic Research for Tomorrow's Technology, Committee on Condensed-Matter and Materials Physics, National Research Council, National Academy Press, Washington, DC, 1999, p. 10.
[9] D.G. Castner, B.D. Ratner, Biomedical surface science: Foundations to frontiers, Surf. Sci. 500 (2002) 28.
[10] M. Fahlman, W.R. Salaneck, Surfaces and interfaces in polymer-based electronics, Surf. Sci. 500 (2002) 904.
[11] B. Kasemo, Biological surface science, Surf. Sci. 500 (2002) 656.
[12] T.H. Rod, J.K. Nørskov, The surface science of enzymes, Surf. Sci. 500 (2002) 678.
[13] S.A. Safran, Statistical thermodynamics of soft surfaces, Surf. Sci. 500 (2002) 127.
[14] M. Tirrell, E. Kokkoli, M. Biesalski, The role of surface science in bioengineered materials, Surf. Sci. 500 (2002) 61.
[15] S.D. Bader, Magnetism in low dimensionality, Surf. Sci. 500 (2002) 172.
[16] J. Shen, J. Kirschner, Tailoring magnetism in artificially structured materials: the new frontier, Surf. Sci. 500 (2002) 300.
[17] J.R. Arthur, Molecular beam epitaxy, Surf. Sci. 500 (2002) 189.
[18] H. Dai, Carbon nanotubes: opportunities and challenges, Surf. Sci. 500 (2002) 218.
[19] H.-J. Freund, Clusters and islands on oxides: from catalysis via electronics and magnetism to optics, Surf. Sci. 500 (2002) 271.
[20] W. Eberhardt, Clusters as new materials, Surf. Sci. 500 (2002) 242.
[21] A.G. Naumovets, Z. Zhang, Fidgety particles on surfaces: how do they jump, walk, group, and settle in virgin areas? Surf. Sci. 500 (2002) 414.
[22] A. Schilling, M. Cantani, J.D. Guo, H.R. Ott, Superconductivity above 130 K in the Hg–Ba–Ca–Cu–O system, Nature 363 (1993) 56.
[23] Correlated Electron Systems, Science 288 (2000).
[24] I.S. Osborn, Science 288 (2000) 438.
[25] R.J. Birgeneau, M.A. Kastner, Frontier physics with correlated electrons, Science 288 (2000) 437.
[26] M. Imada, A. Fujimori, Y. Tokura, Metal–insulator transitions, Rev. Mod. Phys. 70 (1998) 1039–1263;
Y. Tokura, N. Nagaosa, Orbital physics in transition-metal oxides, Science 288 (2000) 462.
[27] V. Kiryukhin, D. Casa, J.P. Hill, B. Keimer, A. Viliante, Y. Tomioka, Y. Tokura, An X-ray-induced insulator-metal transition in a magnetoresistive manganite, Nature 386 (1997) 813.
[28] M. Fiebig, K. Miyano, Y. Tomioka, Y. Tokura, Visualization of the local insulator–metal transition in $Pr_{0.7}Ca_{0.3}MnO_3$, Science 280 (1998) 1925.
[29] H. Oshima, K. Miyano, Y. Konishi, M. Kawasaki, Y. Tokura, Switching behavior of epitaxial perovskite manganite thin films, Appl. Phys. Lett. 75 (1999) 1473.

[30] J. Tranquada, B.J. Sternlieb, J.D. Axe, Y. Nakamura, S. Ushida, Nature 375 (1995) 338;
J. Tranquada, P. Wochner, D.J. Buttery, Phys. Rev. Lett. 78 (1997) 2133.
[31] Workshop on Soft X-ray Science in the Next Millennium: The Future of Photon-In/Photon-Out Experiments, Pikeville, Tennessee, March 15–18, 2000.
[32] J. Orenstein, A.J. Millis, Science 288 (2000) 468.
[33] J. Zaanen, Self-organized one dimensionality, Science 286 (1999) 251.
[34] A. Moreo, S. Yunoki, E. Dagotto, Phase separation scenario for manganese oxides and related materials, Science 283 (1999) 2034.
[35] S.A. Kivelson, E. Fradkin, V.J. Emery, Electronic liquid-crystal phases of a doped Mott insulator, Nature 393 (1998) 550.
[36] P. Littlewood, Phases of resistance, Science 399 (1999) 529.
[37] J. Eroles, G. Ortiz, A.V. Balatsky, A.R. Bishop, Inhomogeneity-induced superconductivity? Europhys. Lett. 50 (2000) 540.
[38] J. Zaanen, Stripes, defeat the Fermi liquid, Nature 404 (2000) 714.
[39] P.W. Anderson, More is different-broken symmetry and nature of hierarchical structure, Science 177 (1972) 393.
[40] 1000 Most Cited Physicists, 1981 to June 1997 (out of over 5,000 examined) http://www.sst.nrel.gov. Current Contents, Research Department, Institute for Scientific Information (ISI).
[41] M.N. Baibich, J.M. Broto, A. Fert, F. Nguyen Van Dau, F. Petroff, P. Eitenne, G. Creuzet, A. Friederich, J. Chazelas, Giant magnetoresistance of (001)Fe/(001) Cr magnetic superlattices, Phys. Rev. Lett. 61 (1988) 2472.
[42] W.E. Pickett, J.S. Moodera, Phys. Today 54 (2001) 39.
[43] D.L. Landau, E.M. Lifshitz, Statistical Physics, Pergamon Press, New York, 1970.
[44] D.R. Nelson, Defect-mediated phase transitions, in: C. Doumb, J.L. Lebowitz (Eds.), Phase Transitions and Critical Phenomena, Academic Press, London, 1983, pp. 1–99.
[45] L.W. Bruch, M.W. Cole, E. Zaremba, Physical Adsorption: Forces and Phenomena, Oxford University Press, Oxford, 1997.
[46] T. Tabata, T. Aruga, Y. Murata, Order–disorder transition on Si(001)-C(4×2) to (2×1), Surf. Sci. 179 (1987) L63–L70.
[47] J.D. Chadi, Atomic and electronic-structures of reconstructed Si(001) surfaces, Phys. Rev. Lett. 43 (1979) 43.
[48] R.M. Tromp, R.J. Hamers, J.E. Demuth, Si(001) dimer structure observed with scanning tunneling microscopy, Phys. Rev. Lett. 55 (1985) 1303;
R.J. Hamers, R.M. Tromp, J.E. Demuth, Scanning tunneling microscopy of Si(001), Phys. Rev. B 34 (1986) 5343.
[49] K. Inoue, Y. Morikawa, K. Terakura, M. Nakayama, Order–disorder phase-transition on the Si(001) surface—critical role of dimer defects, Phys. Rev. B 49 (1994) 14774.
[50] R.A. Wolkow, Direct observation of an increase in buckled dimers on Si(001) at low-temperature, Phys. Rev. Lett. 68 (1992) 2636.
[51] T. Yokoyama, K. Takayanagi, Anomalous flipping motions of buckled dimers on the Si(001) surface at 5 K, Phys. Rev. B 61 (2000) R5078.
[52] Y. Kondo, T. Amakusa, M. Iwatsuki, H. Tokumoto, Phase transition of the Si(001) surface below 100 K, Surf. Sci. 453 (2000) L318.
[53] H. Mutka, Influence of defects and impurities on CDW systems, in: F.W. Boswell, J.C. Bennet (Eds.), Advances in Crystallographic and Microstructural Analysis of Charged Density Waves Modulated Crystals, Kluwer, Dordrecht, 1999.
[54] I. Baldea, M. Badescu, Quasi-regular impurity distribution driven by a charge-density-wave, Phys. Rev. B 48 (1993) 8619.
[55] I. Baldea, M. Apostol, Modulated-imputiy mechansism of pinning in Kcp, J. Phys. C 18 (1985) 6135.
[56] A.W. Overhauser, Exchange and correlation instabilities of simple metals, Phys. Rev. 167 (1968) 691.
[57] G. Gruner, Density Waves in Solids, first ed., Addison-Wesley, Reading MA, 1994.
[58] J.M. Carpinelli, H.H. Weitering, M. Bartkowiak, R. Stumpf, E.W. Plummer, Surface charge ordering transition: α phase of Sn/Ge(111), Phys. Rev. Lett. 79 (1997) 2859.
[59] A.V. Melechko, J. Braun, H.H. Weitering, E.W. Plummer, Two-dimensional phase transition mediated by extrinsic defects, Phys. Rev. Lett. 83 (1999) 999.
[60] A.V. Melechko, J. Braun, H.H. Weitering, E.W. Plummer, The role of defects in two-dimensional phase transitions: an STM study of the Sn/Ge(111) system, Phys. Rev. B 61 (2000) 2235.
[61] H.H. Weitering, A. Melesko, J.M. Carpinelli, J. Zhang, M. Bartkowiak, E.W. Plummer, Defect-mediated condensation of a charge density wave, Science 285 (1999) 2107–2110.
[62] M. Fäth, S. Freisem, A.A. Menovsky, Y. Tomioka, J. Aarts, J.A. Mydosh, Science 285 (1999) 1540.
[63] S.H. Pan, J.P. O'Neal, R.L. Badzey, C. Chamon, H. Ding, J.R. Englebrecht, Z. Wang, H. Eisaki, S. Uchida, A.K. Gukpta, K.-W. Ng, E.W. Hudson, K.M. Lang, J.C. Davis, A microscopic picture of the electronic inhomogeneity in high-T_c superconductor $Bi_2Sr_2CaCu_2O_{8+x}$, in press.
[64] R. Matzdorf, Z. Fang, Ismail, J. Zhang, T. Kimura, Y. Tokura, K. Terakura, E.W. Plummer, Ferromagnetism stabilized by lattice distortion at the surface of the p-wave superconductor Sr_2RuO_4, Science 289 (2000) 746.
[65] Y. Maeno, H. Hashimoto, K. Yoshida, S. Nishizaki, T. Fujita, J.G. Bednorz, F. Lichtenberg, Superconductivity in a layered perovskite without copper, Nature 372 (1994) 532.
[66] T.M. Rice, M. Sigrist, Sr_2RuO_4: an electronic analogue of ^{3}He? J. Phys.: Condens. Matter 7 (1995) L643.
[67] I.I. Mazin, D.J. Singh, Competitions in layered ruthenates: ferromagnetism versus antiferromagnetism and triplet versus singlet pairing, Phys. Rev. Lett. 82 (1999) 4324.

[68] W.E. Pickett, R. Weht, A.B. Shick, Superconductivity in ferromagnetic $RuSr_2GdCu_2O_8$, Phys. Rev. Lett. 83 (1999) 3713.
[69] D.E. Pugel, M.B. Salamon, M.B. Weissman, L.H. Greene, Direct dection of spontaneously broken time-reversal symmetry at surfaces of superconducting $Yba_2Cu_3O_{7-\delta}$, in press.
[70] B.J. Sternlieb, J.P. Hill, U.C. Wildgruber, et al., Charge and magnetic order in $La_{0.5}Sr_{1.5}MnO_4$, Phys. Rev. Lett. 76 (1996) 2169.